EUROPEAN ORGANIZATION FOR NUCLEAR RESEARCH

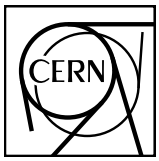

ALICE-PUBLIC-2020-006

Supplemental material: Measurement of the groomed jet radius and momentum splitting fraction in pp and Pb–Pb collisions at $\sqrt{s_{\mathrm{NN}}} = 5.02$ TeV

ALICE Collaboration*

Abstract

This note presents jet substructure measurements in pp and Pb–Pb collisions at $\sqrt{s_{\mathrm{NN}}} = 5.02$ TeV with the ALICE detector. The Soft Drop grooming algorithm provides access to the hard parton splittings inside a jet by removing soft wide-angle radiation. We report the groomed jet momentum fraction, z_{g}, and the (scaled) groomed jet radius, $\theta_{\mathrm{g}} \equiv R_{\mathrm{g}}/R$. Charged-particle jets are reconstructed at midrapidity using the anti-k_{T} algorithm with resolution parameters $R = 0.2$ and $R = 0.4$. In heavy-ion collisions, the large underlying event poses a challenge for the reconstruction of groomed jet observables, since fluctuations in the background can cause groomed parton splittings to be misidentified. By using strong grooming conditions to reduce this background, we report these observables fully corrected for detector effects and background fluctuations for the first time. A narrowing of the θ_{g} distribution in Pb–Pb collisions compared to pp collisions is observed, which provides direct evidence of the modification of the angular structure of jets in the quark–gluon plasma. No significant modification of the z_{g} distribution in Pb–Pb collisions compared to pp collisions is seen. These results are compared with a variety of theoretical models of jet quenching, and provide constraints on jet energy-loss mechanisms and coherence effects in the quark–gluon plasma.

*See Appendix A for the list of collaboration members

1 Introduction

Ultrarelativistic heavy-ion collisions at the Large Hadron Collider (LHC) are used to study the high temperature deconfined phase of strongly interacting matter known as the quark–gluon plasma (QGP) [1–5]. Highly-energetic jets created in the collisions interact with the QGP medium and through those interactions they can lose energy and their internal structure can be modified. This process, known as jet quenching [6–9], can be used to reveal the physical properties of the QGP itself. Previous measurements demonstrate the suppression of jet yields in heavy-ion collisions relative to appropriately scaled pp collisions [10–15], as well as jet substructure modifications [16–18]. These measurements have established that jets undergo energy loss, and that the distribution of momentum of jet constituents is modified relative to that in pp collisions. Some measured observables such as the jet angularity [16] and jet transverse profile [18], which are sensitive to the structure of jets in both angular and momentum space, suggest a narrowing of the jet core in heavy-ion collisions. No direct modification of the intra-jet angular distribution alone has been measured.

Groomed jet substructure in pp collisions allows access to the hard (high-momentum transfer) parton splittings inside a jet by removing soft, wide-angle radiation [19–21]. Groomed jet observables are often under good theoretical control because they can be calculated in perturbative QCD (pQCD) and allow for a controlled reduction of non-perturbative effects. In heavy-ion collisions, groomed jet observables can be used to investigate jet quenching effects in the QGP. Since jet grooming allows access to quantities related to hard splittings in parton showers, it may give a handle on various jet quenching effects such as energy loss, transverse-momentum broadening, path-length dependence and color coherence. Measurements of groomed jet observables in heavy-ion collisions were performed by ALICE and CMS collaborations [22–24], and opened a new avenue in the study of jet substructure in heavy-ion collisions.

In this note, we report results in both pp and Pb–Pb collisions using the Soft Drop (SD) [19–21] grooming algorithm, which identifies a single splitting by first clustering a jet, then reclustering the constituents of that jet using the Cambridge/Aachen (C/A) algorithm [25], and traversing the history of the reclustered tree to identify a particular splitting that satisfies the grooming condition. The groomed splitting is characterized by two kinematic observables: the groomed jet radius, R_{g}, and groomed momentum fraction, z_{g}, as shown in Fig. 1. The groomed jet radius is defined as the angular distance between the two branches of the identified splitting:

$$R_{\mathrm{g}} \equiv \sqrt{\Delta y^2 + \Delta\varphi^2}, \tag{1}$$

where y is the rapidity and φ is the azimuthal angle. In this measurement, we consider the scaled groomed jet radius,

$$\theta_{\mathrm{g}} \equiv \frac{R_{\mathrm{g}}}{R}, \tag{2}$$

where R is the jet resolution parameter used to reconstruct jets in the anti-k_T algorithm, and approximately represents the total angular aperture of the considered jets. The groomed momentum fraction, z_{g}, is defined as the fraction of transverse momentum (p_{T}) carried by the sub-leading (lowest p_{T}) prong in the identified splitting:

$$z_{\mathrm{g}} \equiv \frac{p_{\mathrm{T,subleading}}}{p_{\mathrm{T,leading}} + p_{\mathrm{T,subleading}}}. \tag{3}$$

By measuring both θ_{g} and z_{g} for the same population of jets, one can simultaneously constrain the full kinematic variables of a groomed jet splitting.

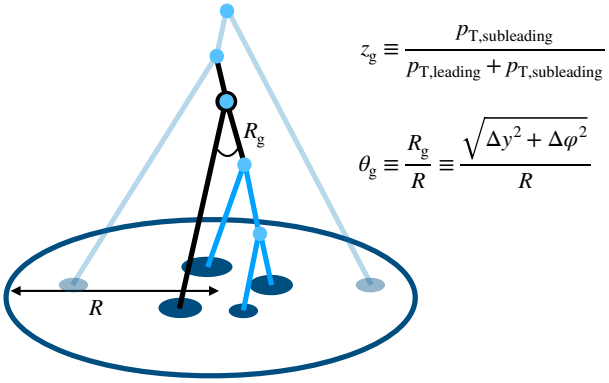

Fig. 1: Graphical representation of the angularly-ordered Cambridge-Aachen reclustering of jet constituents and subsequent Soft Drop grooming procedure [19], with the identified splitting denoted in black and the splittings that were groomed away in light blue.

In pp collisions, measurements of θ_g and z_g distributions test analytical pQCD predictions and constrain the role of non-perturbative effects [26]. Measurements of θ_g and z_g have been performed at RHIC and the LHC [23, 27–30]. At high transverse momentum, the data are described within uncertainties by pQCD predictions [26]. In this note, we report results of θ_g and z_g with stronger grooming parameters than in previous measurements, in which a larger fraction of the jet energy is groomed away.

In heavy-ion collisions, θ_g may be sensitive to multiple jet-quenching physics mechanisms. It was proposed that θ_g can constrain the trade-off between the narrowing of jets due to the relative suppression of gluon-initiated vs. quark-initiated jets, and the broadening of jets due to transverse momentum diffusion [31]. Additionally, θ_g may be sensitive to the ability of the medium to resolve jets via color coherence, where a color dipole may either be resolved by the medium as two independent color charges or remain unresolved as a single color charge, leading to different modifications in the medium [32]. Moreover, uncertainty principle arguments suggest that jet splittings are formed at different times in vacuum ($t_f \sim 1/\theta_g^2$ where t_f is the splitting formation time) such that wider splittings are formed earlier in the parton shower and narrower splittings are formed later. This would result in wider jet splittings traversing on average a longer path in the medium, and undergoing more significant modification of the substructure than narrower jet splittings. Complementary to θ_g, it has been argued that z_g may be sensitive to the modification of the DGLAP splitting function in the QGP, the breaking of color coherence, and the response of the medium to the jet [33–36]. By measuring both θ_g and z_g simultaneously, and thereby both the angular and momentum scales of the hard substructure of jets, these jet-quenching mechanisms can be further constrained.

Up to now, no measurement of θ_g has been performed in heavy-ion collisions. Previous measurements of the z_g distribution by the CMS [22] and ALICE collaborations [23] indicated significant modification with respect to pp collisions for mild grooming settings $z_{cut} = 0.1$ and large-angle splittings $R_g > 0.1$. However, these results were not corrected for background and detector effects, and are difficult to interpret [37]. By using stronger grooming conditions to reduce the splitting background, we report the first fully corrected measurement of groomed substructure observables in heavy-ion collisions, allowing for a rigorous comparison to theoretical calculations.

2 Experimental setup and data sets

A description of the ALICE detector and its performance can be found in Refs. [38, 39]. The pp data set used in this analysis was collected in 2017 during LHC Run 2 at $\sqrt{s} = 5.02$ TeV. A minimum bias (MB) trigger was used, which required a coincidence of hits in V0A and V0C detectors, covering pseudorapidity ranges of $2.8 < \eta < 5.1$ and $-3.7 < \eta < -1.7$, respectively [40]. The Pb–Pb data set was

collected in 2018 during LHC Run 2 at $\sqrt{s_{\rm NN}} = 5.02$ TeV. Central and semi-central triggers that select the 0–10% and 30–50% most central events, based on the multiplicity of produced particles in the forward V0 counters, were used. The centrality was determined using the measured particle multiplicity in the V0 detectors [41, 42]. The event selection includes a primary vertex selection, where the primary vertex is required to satisfy basic quality criteria and to be within 10 cm from the center of the detector. Beam-induced background events were removed using two neutron Zero Degree Calorimeters located ± 112.5 m along the beam axis from the center of the detector. Pileup was rejected based on multiple reconstructed vertices and tracking selections. After these selections, the pp data sample contains 870 million events and corresponds to an integrated luminosity of 18.0 ± 0.4 nb^{-1} [43]. The corresponding Pb–Pb data sample contains 92 million events in central collisions and 90 million events in semi-central collisions, corresponding to an integrated luminosity of 0.12 nb^{-1} and 0.06 nb^{-1}, respectively.

In this analysis, we used charged particle tracks reconstructed using information from both the Time Projection Chamber (TPC) [44] and the Inner Tracking System (ITS) [45]. We define two types of tracks: global tracks and complementary tracks. Global tracks are required to include at least one hit in the silicon pixel detector (SPD) comprising the first two layers of the ITS and to satisfy multiple tracking criteria. Complementary tracks are all those satisfying all the selection criteria of global tracks except for the request of a point in the SPD. They are refitted using the primary vertex to constrain their trajectory in order to preserve a good momentum resolution, especially at high $p_{\rm T}$. Including this second class of tracks ensured approximately uniform azimuthal acceptance, while preserving similar transverse-momentum $p_{\rm T}$ resolution to tracks with SPD hits. Tracks with $0.15 < p_{\rm T} < 100$ GeV/c were accepted over pseudorapidity $|\eta| < 0.9$ and azimuthal angle $0 < \varphi < 2\pi$.

The instrumental performance of the detector was estimated with a model of the ALICE detector and its response to particles using GEANT3 [46]. The tracking efficiency in pp collisions, as estimated with a simulation performed with PYTHIA8 Monash 2013 [47] for the event generation and using the GEANT3 [46] transport code for propagating particles through the simulated ALICE apparatus simulation, is approximately 67% at track $p_{\rm T} = 0.15$ GeV/c, and rises to approximately 84% at $p_{\rm T} = 1$ GeV/c, and remains above 75% at higher $p_{\rm T}$. Studies of the centrality dependence of the tracking efficiency in a HIJING [48] simulation demonstrated that the tracking efficiency is approximately 2% lower in 0–10% central Pb–Pb collisions compared to pp collisions, independent of track $p_{\rm T}$. The momentum resolution $\sigma(p_{\rm T})/p_{\rm T}$ was estimated from the covariance matrix of the track fit [39], and is approximately 1% at track $p_{\rm T} = 1$ GeV/c and 4% at $p_{\rm T} = 50$ GeV/c.

3 Analysis method

3.1 Jet reconstruction

Jets are reconstructed from charged tracks with FastJet 3.2.1 [49] using the anti-$k_{\rm T}$ algorithm with E-scheme recombination for resolution parameters $R = 0.2$ and $R = 0.4$ [50, 51]. The pion mass is assumed for all jet constituents. Jets in heavy-ion collisions have a large uncorrelated background contribution due to fluctuations in the underlying event (UE). In ALICE, the UE contribution is quantified through the transverse momentum density per unit area, ρ, which is on average 146 GeV/c in central collisions and 32.3 GeV/c in semi-central collisions. In this measurement the event-by-event constituent subtraction method is used, which corrects the overall jet $p_{\rm T}$ and its substructure simultaneously by subtracting energy constituent by constituent [52, 53]. The constituent subtraction method works by adding infinitesimally small "ghosts" to the event over the entire acceptance whose transverse momentum is negative. The ghosts and particles are then combined based on how close they are to each other, as defined by

$$\Delta R = {p_{\rm T}}^{\alpha} \sqrt{(\eta - \eta_{\rm g})^2 + (\varphi - \varphi_{\rm g})^2} \tag{4}$$

where η_g and φ_g are the η and φ of the ghosts, p_T is the transverse momentum of the particle and α is a parameter that can be varied. Particles and ghosts with less than zero total momentum are removed from the event. The maximum recombination distance R_{max} specifies how close the particles and ghosts need to be to be considered a match. In this note, we considered $R_{max} = 0.25$ and $\alpha = 0$, which leads to an unbiased corrected charged-particle jet transverse momentum $p_{T,\,ch\,jet}$. After background subtraction, the measured range is $40 < p_{T,\,ch\,jet} < 120$ GeV/c. The jet axis is required to be within the fiducial volume of the TPC, $|\eta_{jet}| < 0.9 - R$, where η_{jet} is the jet pseudorapidity. The jet must not contain a track with p_T above 100 GeV/c in order to optimize the overall jet momentum resolution.

The jet reconstruction performance is studied by comparing PYTHIA8 generated jets at "truth level" (before the particles undergo interactions with the detector) to those at "detector level" (after the ALICE GEANT3 detector simulation). In pp collisions we construct two collections of jets: pp truth level (PYTHIA truth) and pp detector level (PYTHIA with detector simulation). We then geometrically match the detector-level jets with truth-level jets within $\Delta R < 0.6\,R$. In Pb–Pb collisions, we embed PYTHIA8 events into 0–10% or 30–50% centrality Pb–Pb measured events. We then assign a truth-level jet from PYTHIA with an associated "combined" jet consisting of a jet constructed from PYTHIA detector level tracks and Pb–Pb tracks. To define such a match, we construct three collections of jets: pp truth level and pp detector level (in the same way as in pp collisions) and "combined". We use a scheme of jet matching where we match the "combined" jet geometrically to the nearest pp detector-level jet, and require that the jets are within $\Delta R < 0.6R$ and that the combined jet contains at least 50% of the total track p_T of the pp-detector level jet, implicitly enforcing uniqueness. Additionally, the pp detector-level jet is matched to its corresponding pp truth-level jet in the same way as was done for the jets in pp collisions.

We perform Soft Drop grooming [19], in which we re-cluster each jet with the Cambridge-Aachen algorithm with resolution parameter R, and then decluster the jet starting from the largest-angle splitting, where each splitting in the declustered sequence is defined by $z \equiv \frac{p_{T,\text{subleading}}}{p_{T,\text{leading}}+p_{T,\text{subleading}}}$. If

$$z < z_{cut}\theta^{\beta}, \tag{5}$$

where $\theta \equiv \frac{\Delta R}{R} \equiv \frac{\sqrt{\Delta y^2+\Delta\varphi^2}}{R}$ and z_{cut}, β are tunable free parameters of the grooming algorithm, then we drop the softer branch and proceed to the next splitting in the harder branch. If

$$z > z_{cut}\theta^{\beta}, \tag{6}$$

then we conclude the grooming procedure, with all remaining constituents defining the groomed jet. The groomed jet radius and groomed momentum fraction are then defined according to Eqs. (1)–(3) and in this analysis we use $\beta = 0$.

Local background fluctuations in a heavy-ion environment can result in an incorrect splitting being identified by the grooming algorithm, in which the reconstructed splitting is unrelated to a hard process. In order to address this issue, this measurement has been performed by applying strong grooming conditions, $z_{cut} = 0.2$ and 0.4 (with $\beta = 0$), which better mitigates these effects compared to milder grooming conditions such as $z_{cut} = 0.1$ [37]. The background subtraction technique was improved by using the event-by-event constituent subtraction method instead of the jet-by-jet constituent subtraction method [52, 53], which was used in previous ALICE jet-shape and jet-substructure measurements [16–18, 23]. Additionally, by also measuring jets with a small resolution parameter ($R = 0.2$ instead of $R = 0.4$), the magnitude of these prong-mistagging effects was further decreased, since the collinear jet fragmentation enhances the fraction of signal jet energy compared to background energy density. Finally, the analysis for jets with a resolution parameter of $R = 0.4$ was also performed in more peripheral collisions (30–50% instead of 0–10%), where the impact of the background is less relevant.

In order to evaluate the rate of prong mistagging due to the residual background effects, we performed a study to quantify the subleading prong purity by embedding jets simulated with the PYTHIA8 event generator [47] into measured Pb–Pb data, defined as the probability for subleading prongs at the pp detector level get reconstructed inside the subleading prong after the embedding procedure. To do so, we tagged prongs at the detector level according to the manner in which they were reconstructed in the embedded event. This was done by checking if 50% of the p_{T} in the detector-level prong ended up in either of the prongs in the embedded event. The residual background contribution ranges from approximately 5% up to 15% at lower p_{T}, in more central events, and at larger R. This level of background contamination is small enough to allow the results to be unfolded for detector effects and background fluctuations. The impact of the residual background contribution is quantified in Section 4, and remains one of the leading sources of systematic uncertainty.

3.2 Unfolding

The reconstructed $p_{\mathrm{T,\,ch\,jet}}$, θ_{g}, and z_{g} differ from their true values due to tracking inefficiency, particle-material interactions, and track p_{T} resolution. Moreover, in Pb–Pb collisions, background fluctuations significantly smear the reconstructed distributions of θ_{g} and z_{g}. To account for these effects, we simulated events with the PYTHIA8 generator [47] using the Monash 2013 tune and the GEANT3 model [46] for the particle transport in the ALICE detector material. We constructed a 4D response matrix (RM) that describes the detector and background response in $p_{\mathrm{T,\,ch\,jet}}$ and θ_{g} or z_{g}: $R\left(p^{\mathrm{det}}_{\mathrm{T,\,ch\,jet}}, p^{\mathrm{truth}}_{\mathrm{T,\,ch\,jet}}, \theta_{\mathrm{g}}^{\mathrm{det}}, \theta_{\mathrm{g}}^{\mathrm{truth}}\right)$, where $p^{\mathrm{det}}_{\mathrm{T,\,ch\,jet}}$ is the detector-level $p_{\mathrm{T,\,ch\,jet}}$ in the case of pp collisions or the "combined" jet after embedding in the case of Pb–Pb collisions and $p^{\mathrm{truth}}_{\mathrm{T,\,ch\,jet}}$ is the truth-level $p_{\mathrm{T,\,ch\,jet}}$, and analogously for z_{g}. We then perform a 2D unfolding in $p_{\mathrm{T,\,ch\,jet}}$ and θ_{g} or z_{g} using the iterative Bayesian unfolding algorithm [54] implemented in the RooUnfold package [55].

We impose a lower p_{T} limit on the data that is input to the unfolding, in order to reject combinatorial jets. For $R = 0.2$ jets in 0–10% centrality and $R = 0.4$ in 30–50% centrality, we limit the input range to $p^{\mathrm{det}}_{\mathrm{T,\,ch\,jet}} \in [40, 120]$ GeV/c. Similarly for $R = 0.4$ jets in 0–10% centrality, we limit the input range to $p^{\mathrm{det}}_{\mathrm{T,\,ch\,jet}} \in [60, 140]$ GeV/c. No such limitation is imposed on $p^{\mathrm{truth}}_{\mathrm{T,\,ch\,jet}}$ during the unfolding process. The distributions after unfolding are then corrected for the kinematic efficiency, defined as the efficiency of reconstructing a "true" jet at a particular $p^{\mathrm{truth}}_{\mathrm{T,\,ch\,jet}}$ value given a reconstructed jet $p^{\mathrm{det}}_{\mathrm{T,\,ch\,jet}}$ range. This inefficiency can result from background effects including smearing from the SD threshold and p_{T}-smearing of the jet out of the selected $p_{\mathrm{T,\,ch\,jet}}$ range. The kinematic efficiency is 70% or higher in all cases for $p_{\mathrm{T,\,ch\,jet}} > 60$ GeV/c. Since the final observables are normalized per jet, the kinematic efficiency only affects the shape of the distribution. We include the number of untagged jets in the unfolding procedure as an additional bin adjacent to the lower edge of the θ_{g} and z_{g} distributions (in iterative Bayesian unfolding, the arrangement of the bins is immaterial). The number of iterations, which sets the strength of regularization, is chosen by minimizing the quadrature sum of the statistical and systematic unfolding uncertainties or by checking that the unfolding closure tests described below are successful. This results in the optimal number of iterations ranging from 3 to 6.

To validate the performance of the unfolding procedure, we perform refolding tests, in which the RM is multiplied by the unfolded solution and compared to the original detector-level spectrum. We also do closure tests, in which the shape of the input MC spectrum is modified to account for the fact that actual distribution may be different than the MC input spectrum. In all cases, we achieve closure within statistical uncertainties. Additionally, we perform a thermal closure test to quantify the sensitivity of the final result to combinatorial jets and background splittings. This consisted of redoing the entire analysis on "combined" events containing a PYTHIA event and a thermal background, in which "combined" jets were clustered from the combination of PYTHIA detector-level particles and thermal background particles. The background was modeled by generating N particles with p_{T} taken from a Gamma distribution, $f_{\Gamma}(p_{\mathrm{T}}; \beta) \propto p_{\mathrm{T}} e^{-p_{\mathrm{T}}/\beta}$, where N and β were fixed to roughly fit the $R = 0.2$ δp_{T} distribution in Pb–Pb

data [56]. This background model was verified to describe the subleading prong purity to percent-level accuracy. The test consisted of constructing the combined detector-level jet spectrum, building the RM, unfolding the combined jets – and comparing the spectrum to the truth-level PYTHIA spectrum. Since the background does not have any jet component, this test is able to quantify the extent to which the analysis procedure indeed recovers the signal distribution and is not contaminated by background. Due to a residual contamination of mistagged splittings, non-closure is observed in some distributions and is therefore incorporated as a systematic uncertainty, which is discussed further in Section 4.

4 Systematic uncertainties

The systematic uncertainties in this measurement are due to the tracking efficiency, the unfolding procedure, residual mistagged prongs, the background subtraction procedure, and the generator model-depdenence. Tables 1 and 2 summarizes the systematic uncertainty contributions for Pb–Pb and pp collisions, respectively. All sources of systematic uncertainty contribute significantly in certain regions of the measured observables. The total systematic uncertainty is calculated as the quadratic sum of all of the individual systematic uncertainties described below.

The systematic uncertainty due to the uncertainty of the tracking efficiency is evaluated using random rejection of additional tracks in jet finding according to the estimated tracking efficiency uncertainty of 4%, based on variations in the track selection criteria and on the ITS-TPC track-matching efficiency uncertainty. In order to assign a systematic uncertainty to the final result, we construct an alternative response matrix by randomly rejecting an additional 4% of tracks in jet finding. This response matrix is then used to unfold the same measured result as used in the final result. This result is compared to the main result, with the differences in each bin taken as the systematic uncertainty.

We perform several systematic variations on the unfolding procedure to evaluate a shape systematic uncertainty arising from the unfolding regularization procedure:

- The number of iterations in the unfolding procedure was varied by ± 2 units and the difference with respect to the nominal result is taken as the systematic uncertainty.
- The prior distribution is scaled by variations larger than that expected in the data. The difference between the result unfolded with this RM and the original is taken as the systematic uncertainty.
- The binnings in the θ_g and z_g were varied to be finer and coarser than the nominal binning.
- The lower bound in the detector level charged-particle jet transverse momentum $p_{T,\,\mathrm{ch\,jet}}^{\mathrm{det}}$ range was extended up and down by 5 GeV/c.

The constituent subtraction introduces a bias in the observed distributions, since it implicitly makes a choice of how much p_T to subtract from soft particles compared to the hard particles, and similarly for their angular distributions. To estimate the size of the corresponding systematic uncertainty, we vary R_{max} from "under-subtraction" ($R_{\mathrm{max}} = 0.05$) to "over-subtraction" ($R_{\mathrm{max}} = 0.7$), around the nominal value of $R_{\mathrm{max}} = 0.25$. We take the maximum deviation of these two variations as the systematic uncertainty.

There is a small but potentially significant number of mistagged splittings that remain in the raw distributions. In principle, the unfolding procedure corrects for any mistagged splittings, however this procedure is imperfect. To quantify the systematic uncertainty due to residual mistagged splittings, we take the bin-by-bin non-closure of the thermal model closure test described in Section 3. This introduces some model-dependence of the background but still reasonably quantifies the extent of the remaining background contribution. We also consider the non-closure derived by weighting the input distribution in the MC to be similar to the shape in the Pb–Pb data, unfolding with the unweighted response, and comparing

Pb–Pb	Relative uncertainty (%)					
	Trk. eff.	Unfolding	Generator	Tagging	Bkgd. sub.	Total
z_g						
0–10% $R = 0.2$	1–4%	1–4%	1–7%	1–2%	1–6%	4–10%
0–10% $R = 0.4$	1–13%	1–4%	1–7%	2–26%	4–28%	9–41%
30–50% $R = 0.4$	0–2%	0–5%	1–7%	1–6%	2–5%	5–9%
θ_g						
0–10% $R = 0.2$	1–8%	1–4%	1–5%	1–19%	1–14%	3–24%
30–50% $R = 0.4$	3–6%	1–7%	1–5%	0–4%	2–15%	6–15%
30–50% $R = 0.4$ $z_{cut} = 0.4$	4–11%	2–11%	1–5%	1–5%	1–13%	4–20%

Table 1: Summary of systematic uncertainties on the Pb–Pb measurements. The ranges correspond to the minimum and maximum systematic uncertainties obtained. All values correspond to $z_{cut} = 0.2$ unless otherwise noted.

pp	Relative uncertainty (%)			
	Trk. eff.	Unfolding	Generator	Total
z_g				
$R = 0.2$	0–3%	2–4%	2–4%	3–6%
$R = 0.4$	0–3%	0–6%	0–3%	1–7%
θ_g				
$R = 0.2$	1–5%	2-5%	1–3%	4–6%
$R = 0.4$	1–5%	0–10%	0–5%	2–13%
$R = 0.4$ $z_{cut} = 0.4$	1–15%	2–9%	0–13%	3–17%

Table 2: Summary of systematic uncertainties on the pp measurements. The ranges correspond to the minimum and maximum systematic uncertainties obtained. All values correspond to $z_{cut} = 0.2$ unless otherwise noted.

to the weighted truth-level distribution. In cases where this non-closure is larger than the non-closure obtained from the thermal closure test, we use this second non-closure as a systematic uncertainty.

A systematic uncertainty associated with the model-dependent reliance on the Monte Carlo generator which is used to unfold the spectra is included. We construct a fast simulation to parameterize the tracking efficiency and track p_T resolution, and build response matrices using PYTHIA8 Monash 2013 and either Herwig7 [57] (in the pp case) or JEWEL 2.2.0 [58] (in the Pb–Pb case) as generators. For Herwig7, we use the default tune, and for JEWEL, we use settings described in Ref. [59] with no recoils. Even though a full detector simulation using PYTHIA8 has also been generated, a fast simulation is used for this purpose so that there is complete parity between the two generators in the calculation of this systematic uncertainty. These two response matrices are then used to unfold the measured data, and the differences between the two unfolded results in each interval are taken as a symmetric uncertainty.

5 Results

We report the z_g and θ_g distributions in bins of $p_{T,\,\mathrm{ch\,jet}}$ between 60 and 100 GeV/c for $z_{cut} = 0.2$ in central (0–10%) and semicentral (30–50%) Pb–Pb collisions. In addition, in semicentral events we present the distributions for $z_{cut} = 0.4$. The measurements are reported for $R = 0.2$ and $R = 0.4$. The distributions are reported as normalized differential cross sections,

$$\frac{1}{\sigma_{\mathrm{jet,inc}}}\frac{\mathrm{d}\sigma}{\mathrm{d}z_g} \equiv \frac{1}{N_{\mathrm{jet,inclusive}}}\frac{\mathrm{d}N}{\mathrm{d}z_g}, \tag{7}$$

where N is the number of jets passing the Soft Drop condition in a given event sample with a given $p_{T,\,\mathrm{ch\,jet}}$, $N_{\mathrm{jet,inclusive}}$ is the number of inclusive jets in the same sample, and $\sigma, \sigma_{\mathrm{jet,inc}}$ are the corresponding cross sections. The analog of Eq. (7) defined for z_g applies for θ_g.

The z_g distributions are shown in Fig. 2 (for central Pb–Pb collisions) and Fig. 3 (for the semicentral collisions). The θ_g distributions are shown in Fig. 4 (for central Pb–Pb collisions) and Fig. 5 (for the semicentral collisions). The distributions from Pb–Pb collisions are compared with the corresponding distributions from pp collisions, with their ratios displayed in the bottom panels. The relative uncertainties are assumed to be uncorrelated between pp and Pb–Pb collisions, and are added in quadrature in the ratio. In Pb–Pb collisions the precision of the measurements decreases as the jet resolution parameter is increased or the centrality is decreased, as the prong mis-tagging probability decreases with centrality and with decreasing R.

The fraction of jets that do not contain a splitting that passes the Soft Drop condition (f_{tagged}) ranges from 10–12% for $z_{\mathrm{cut}} = 0.2$ and is 44% for $z_{\mathrm{cut}} = 0.4$. The differences in these tagging rates between pp and Pb–Pb are at most 2%. Since these differences between pp and Pb–Pb collisions are small, the measured distributions are approximately self-normalized, and therefore any modifications in Pb–Pb compared to pp can change the shape of the distribution, but keep the integral approximately the same.

5.1 Comparing pp and Pb–Pb collisions

We find that the z_g distributions in Pb–Pb collisions are consistent with those in pp collisions within the experimental uncertainties. This holds independent of the jet momentum, jet resolution parameter, or centrality of the Pb–Pb collisions. These measurements provide a benchmark for theoretical description of the jet-medium interactions, constraining the in-medium modifications of the momentum structure of the hard splittings to be less than 10% to 20% depending on the jet R and collision centrality.

The situation is remarkably different when comparing the groomed jet radius in both systems. For $R = 0.2$ in central collisions, the data suggests a narrowing of the Pb–Pb distribution relative to the pp distribution is observed (see Fig. 4). The apparent narrowing of jets persists even in semicentral Pb–Pb collisions for $R = 0.4$ (see Fig. 5) where in general quenching effects are expected to be less than in the most central collisions. In the semicentral case, we also explored the dependence of the large-angle suppression on the shared momentum fraction of the splitting for two values of z_{cut} (see $z_{\mathrm{cut}} = 0.4$ in the right panel of Fig. 5).

5.2 Comparison to theoretical models

We compare the ratio of the measurements in pp and Pb–Pb collisions to several theoretical implementations of jet quenching.

JETSCAPE. The prediction by the JETSCAPE Collaboration [60] is extracted from a Monte Carlo implementation of multi-stage energy loss with the MATTER [64] medium-modified parton shower model controlling the high-virtuality phase and the Linear Boltzmann Transport (LBT) model [65] describing the low-virtuality phase. The version of JETSCAPE used for this calculation employs a jet transport coefficient, $\hat{q}$, that includes dependence on parton virtuality, in addition to dependence on the local temperature and running of the parton-medium coupling. The JETSCAPE prediction reproduces the measurements well.

JEWEL. The prediction by JEWEL [58, 66] is a Monte Carlo implementation of BDMPS-based medium-induced gluon radiation in a medium modeled with a Bjorken expansion. We use JEWEL 2.2.0 with an initial temperature $T_i = 590$ MeV and initial quenching time $\tau_i = 0.4$, which provides an accurate description of a variety of jet quenching observables [59]. We consider the impact of medium recoil by including results both with and without recoils enabled. In the case with recoils included, we perform a subtraction of the thermal component of the recoils by using the constituent subtraction algorithm.

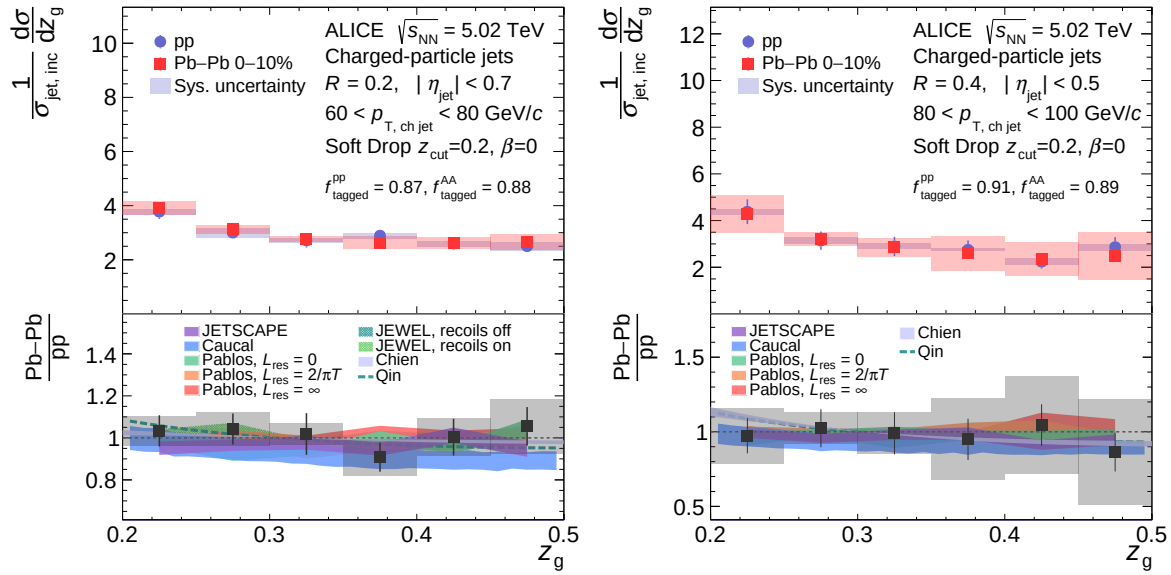

Fig. 2: Unfolded z_g distributions for charged-particle jets in 0–10% central Pb–Pb collisions compared to pp collisions for $R = 0.2$ (left) and $R = 0.4$ (right). The distributions are normalized to the inclusive jet cross section in the $p_{T,\,ch\,jet}$ interval, and f_{tagged} indicates the fraction of splittings that were tagged to pass the SD condition in the selected $p_{T,\,ch\,jet}$ interval. The ratios in the bottom panel are compared to the following theoretical predictions: JETSCAPE [60], Caucal et al. [34, 61], Chien et al. [33], Qin et al. [35], and Pablos et al. [36, 62, 63]. The predictions by Caucal et al. are performed for $75 < p_{T,\,jet} < 100$ GeV/c for $R = 0.2$ and $100 < p_{T,\,jet} < 130$ GeV/c for $R = 0.4$. The predictions by Chien et al. are performed for $100 < p_{T,\,jet} < 130$ GeV/c for $R = 0.2$ and $130 < p_{T,\,jet} < 160$ GeV/c for $R = 0.4$. The predictions by Qin et al. are performed for $90 < p_{T,\,jet} < 120$ GeV/c for $R = 0.2$ and $120 < p_{T,\,jet} < 150$ GeV/c for $R = 0.4$.

Caucal et al. The prediction by Caucal et al. [34, 61] implements a pQCD parton shower with incoherent interactions including both factorized vacuum and medium-induced emissions in a static brick medium. The model describes the trend found in the data well – suggesting that the constituents of the (vacuum) shower once implanted into the medium act as independent emitters.

Chien et al. The prediction by Chien et al. [33] (for z_g only) applies Soft Collinear Effective Theory with Glauber gluon interactions. The prediction describes the z_g measurements well.

Qin et al. The prediction by Qin et al. [35] (for z_g only) applies the higher twist formalism with the assumption of coherent energy loss. The prediction describes the z_g measurements well.

Pablos et al. The prediction by Pablos et al. [36, 62, 63], known as the Hybrid Model, consists of partons produced by a vacuum shower that interact with the medium according to a strongly-coupled AdS/CFT-based model. In the Hybrid Model, the parameter L_{res} describes the degree to which the medium can resolve the jet angular structure, where $L_{res} = 0$ corresponds to full resolution of all jet constituents (fully incoherent), $L_{res} = \infty$ corresponds to fully coherent energy loss, and $L_{res} = 2/\pi T$ corresponds to coherence at scales less than $2/\pi T$ and incoherence at scales above $2/\pi T$, where T is the local medium temperature. For each value of L_{res}, the quenching parameter κ is separately tuned to achieve equivalent energy loss in all cases. The data favor the incoherent energy loss ($L_{res} = 0$) supporting a picture where the emitted gluons interact independently with the medium once they are sufficiently apart/de-cohered.

Yuan et al. The predictions by Yuan et al. [31] consist of two different types of calculations, both only for θ_g. The calculations labeled "med q/g" and "quark" consist of θ_g distributions where only the medium-modified quark-gluon fractions are varied, without any additional effects (corresponding to fully coherent energy loss). The medium quark-gluon fractions in the "med q/g" case are taken from a

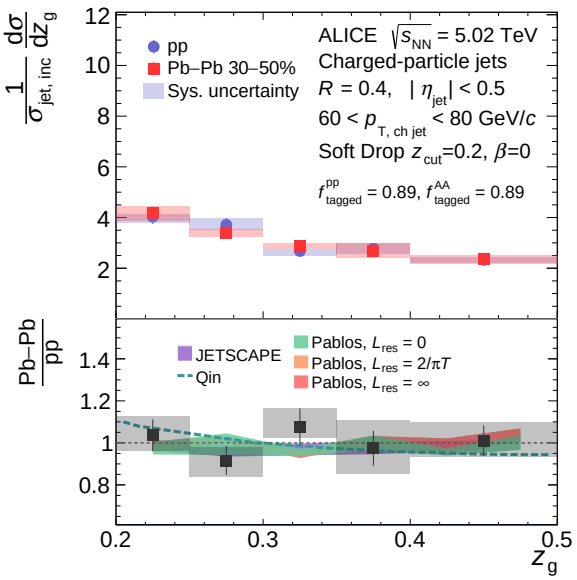

Fig. 3: Unfolded z_g distribution for charged-particle jets in 30–50% Pb–Pb collisions in red compared to pp collisions for $R = 0.4$. The distributions are normalized to the inclusive jet cross section in the $p_{T,\text{ch jet}}$ interval, and f_{tagged} indicates the fraction of splittings that were tagged to pass the SD condition in the selected $p_{T,\text{ch jet}}$ interval. The ratios in the bottom panel are compared to the following theoretical predictions: JETSCAPE [60], Qin et al. [35] and Pablos et al. [36, 62, 63]. The prediction by Qin et al. is performed for $90 < p_{T,\text{jet}} < 120\,\text{GeV}/c$.

global analysis of jet quenching data in Ref. [67], with a relative suppression factor of approximately four between gluon jets and quarks jets, and the "quark" case is a quark only model where the gluon jets are completely suppressed by the medium (to show the maximum possible impact of this mechanism – which is disfavored by comparisons to jet R_{AA}). The calculation labeled "$\hat{q}L$" includes an implementation of transverse momentum broadening. The latter is rejected by the data, whereas the calculations pointing towards strong modifications of the quark-to-gluon ratio in Pb–Pb collisions reproduce the narrowing reasonably well. This prompts further investigations of quenching effects targeting exclusive studies for quark and gluon induced jets in Pb–Pb collisions [16, 68].

The Pb–Pb-to-pp ratios of z_g distributions are well described by all theoretical predictions considered. The modifications, which have been constrained by previous measurements [22, 23], are predicted to be small, and the differences between them are yet smaller than the current uncertainty on the data. Nevertheless, these new measurements provide the first direct comparisons of predictions to fully corrected data, and limit the possible z_g modifications to 10–20% depending on the centrality, jet R, and the grooming settings considered.

Despite employing different microscopic implementations of the jet-medium interactions, the majority of the models capture the qualitative feature of the narrowing seen in the θ_g distributions. However, in a number of ways they provide new insight to the nature of the modifications, as outlined in the following section, and indicate promising directions for further studies.

5.3 Discussion

The theoretical models can be grouped according to three distinct mechanisms by which θ_g is modified: incoherent energy loss, coherent energy loss, and transverse broadening. The measurements are consistent with models implementing (transverse) *incoherent* interaction of the jet shower constituents with the medium. This is well illustrated by calculations of Pablos et al. and supported by Caucal et al., JEWEL,

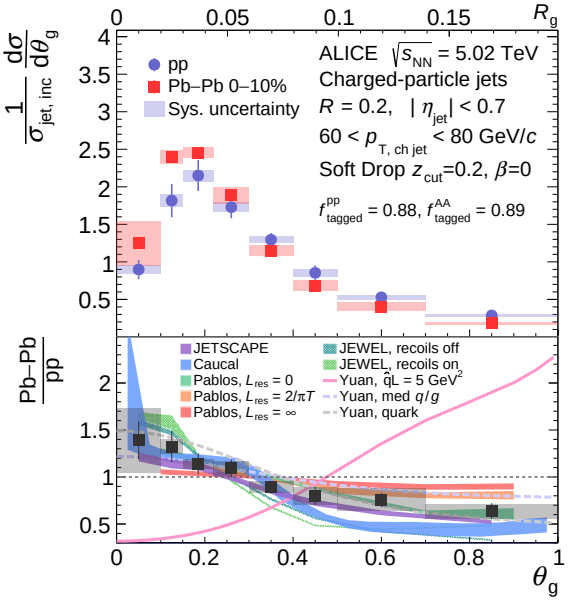

Fig. 4: Unfolded θ_g distributions for charged-particle jets in 0–10% central Pb–Pb collisions compared to pp collisions for $R = 0.2$. The distributions are normalized to the inclusive jet cross section in the $p_{T,\text{ch jet}}$ interval, and f_{tagged} indicates the fraction of splittings that were tagged to pass the SD condition in the selected $p_{T,\text{ch jet}}$ interval. The ratios in the bottom panel are compared to the following theoretical predictions: JETSCAPE [60], Caucal et al. [34, 61], Pablos et al. [36, 62, 63], and Yuan et al. [31]. The predictions by Caucal et al. are performed for $75 < p_{T,\text{jet}} < 100$ GeV/c.

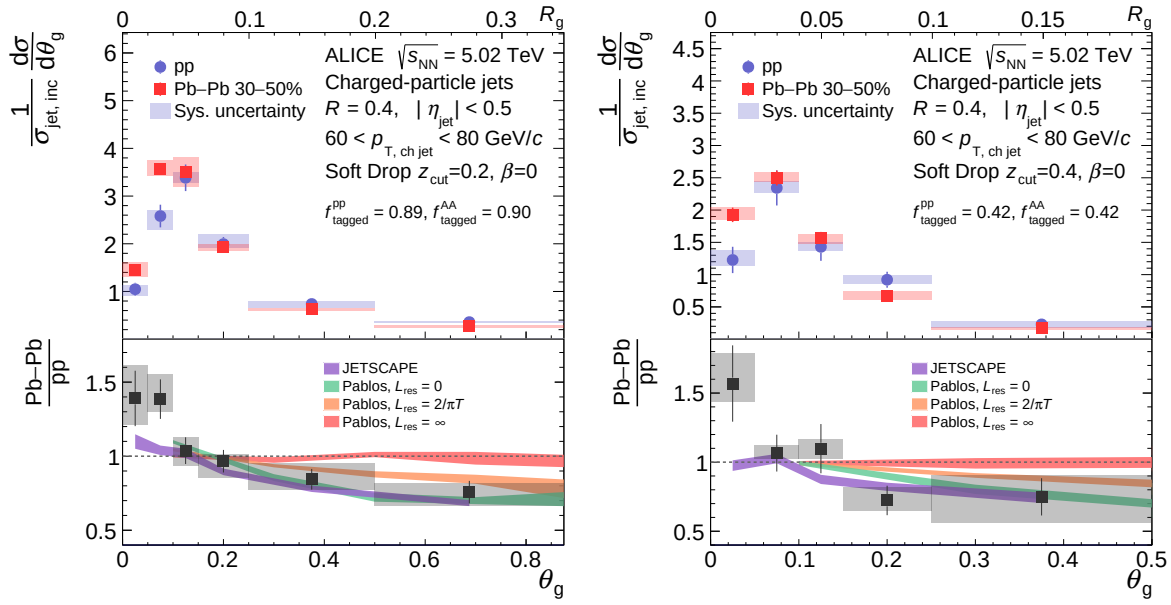

Fig. 5: Unfolded θ_g distributions for charged-particle jets in 30–50% Pb–Pb collisions compared to pp collisions for $R = 0.4$. The distributions are normalized to the inclusive jet cross section in the $p_{T,\text{ch jet}}$ interval, and f_{tagged} indicates the fraction of splittings that were tagged to pass the SD condition in the selected $p_{T,\text{ch jet}}$ interval. The left panel is for a SD grooming $z_{cut} = 0.2$ and the right panel is for $z_{cut} = 0.4$. The ratios in the bottom panel are compared to the following theoretical predictions: JETSCAPE [60] and Pablos et al. [36, 62, 63].

and JETSCAPE. It was shown that in vacuum, using Pythia simulations [36], a large R_g correlates with high intra-jet multiplicity. In the models where the amount of energy lost by the jet in the medium de-

pends on the number of sources from the vacuum shower, the suppression of large-R_g jets is naturally explained. On the other hand, the Yuan et al. calculation with medium-modified "quark/gluon" fractions indicate that the data could be explained by the stronger suppression of on average broader and more abundant splittings in gluon showers, with fully coherent energy loss. These two physics mechanisms – the degree of incoherent energy loss, and the relative quark/gluon suppression – both lead to a suppression of wide-angle splittings. The prediction by Yuan et al. "$\hat{q}L$" exhibits the opposite trend compared to the data, demonstrating that there is no strong transverse broadening in the hard substructure.

In qualitative terms, disregarding the differences in actual parton shower implementations between the models, the agreement with data depends on the physical properties of the medium. The presented measurements of the angular structure clearly indicate that the medium has a significant resolving power for splittings with a particular dependence on the angular (or coherence) scale promoting narrow structures and/or filtering out (via quenching) the "wide" splits in groomed jets or wider jets altogether.

6 Conclusion

We have measured the groomed jet momentum fraction, z_g, and the (scaled) groomed jet radius, θ_g, of charged-particle jets in pp and Pb–Pb collisions at $\sqrt{s_{NN}} = 5.02$ TeV with the ALICE detector. By using stronger grooming conditions in the Soft Drop grooming algorithm, we suppressed contamination of mistagged splittings from the underlying event, and unfolded the final distributions for detector and background fluctuation effects. This allows for the first time the direct comparison of groomed jet measurements in heavy-ion collisions with theoretical predictions of jet quenching in the quark–gluon plasma. The z_g distributions are consistent with no modification in Pb–Pb collisions compared to pp collisions. The θ_g distributions are narrower in Pb–Pb collisions compared to pp collisions, which is the first direct experimental evidence for the modification of the angular scale of groomed jets in heavy-ion collisions.

These new results demonstrate sensitivity to the microscopic structure of the QGP, including its angular resolving power. This marks an important step towards quantitative understanding of the properties of the QGP and provides a new path for novel differential jet substructure measurements to further elucidate the microscopic nature of the QGP.

Acknowledgements

We gratefully acknowledge Paul Caucal, Yang-Ting Chien, Daniel Pablos, Chanwook Park, Guang-You Qin, Gregory Soyez, Feng Yuan, and the JETSCAPE Collaboration for providing theoretical predictions. We thank Korinna Zapp for discussions regarding recoil subtraction in the JEWEL model.

The ALICE Collaboration would like to thank all its engineers and technicians for their invaluable contributions to the construction of the experiment and the CERN accelerator teams for the outstanding performance of the LHC complex. The ALICE Collaboration gratefully acknowledges the resources and support provided by all Grid centres and the Worldwide LHC Computing Grid (WLCG) collaboration. The ALICE Collaboration acknowledges the following funding agencies for their support in building and running the ALICE detector: A. I. Alikhanyan National Science Laboratory (Yerevan Physics Institute) Foundation (ANSL), State Committee of Science and World Federation of Scientists (WFS), Armenia; Austrian Academy of Sciences, Austrian Science Fund (FWF): [M 2467-N36] and Nationalstiftung für Forschung, Technologie und Entwicklung, Austria; Ministry of Communications and High Technologies, National Nuclear Research Center, Azerbaijan; Conselho Nacional de Desenvolvimento Científico e Tecnológico (CNPq), Financiadora de Estudos e Projetos (Finep), Fundação de Amparo à Pesquisa do Estado de São Paulo (FAPESP) and Universidade Federal do Rio Grande do Sul (UFRGS), Brazil; Ministry of Education of China (MOEC) , Ministry of Science &

Technology of China (MSTC) and National Natural Science Foundation of China (NSFC), China; Ministry of Science and Education and Croatian Science Foundation, Croatia; Centro de Aplicaciones Tecnológicas y Desarrollo Nuclear (CEADEN), Cubaenergía, Cuba; Ministry of Education, Youth and Sports of the Czech Republic, Czech Republic; The Danish Council for Independent Research | Natural Sciences, the VILLUM FONDEN and Danish National Research Foundation (DNRF), Denmark; Helsinki Institute of Physics (HIP), Finland; Commissariat à l'Energie Atomique (CEA) and Institut National de Physique Nucléaire et de Physique des Particules (IN2P3) and Centre National de la Recherche Scientifique (CNRS), France; Bundesministerium für Bildung und Forschung (BMBF) and GSI Helmholtzzentrum für Schwerionenforschung GmbH, Germany; General Secretariat for Research and Technology, Ministry of Education, Research and Religions, Greece; National Research, Development and Innovation Office, Hungary; Department of Atomic Energy Government of India (DAE), Department of Science and Technology, Government of India (DST), University Grants Commission, Government of India (UGC) and Council of Scientific and Industrial Research (CSIR), India; Indonesian Institute of Science, Indonesia; Istituto Nazionale di Fisica Nucleare (INFN), Italy; Institute for Innovative Science and Technology , Nagasaki Institute of Applied Science (IIST), Japanese Ministry of Education, Culture, Sports, Science and Technology (MEXT) and Japan Society for the Promotion of Science (JSPS) KAKENHI, Japan; Consejo Nacional de Ciencia (CONACYT) y Tecnología, through Fondo de Cooperación Internacional en Ciencia y Tecnología (FONCICYT) and Dirección General de Asuntos del Personal Academico (DGAPA), Mexico; Nederlandse Organisatie voor Wetenschappelijk Onderzoek (NWO), Netherlands; The Research Council of Norway, Norway; Commission on Science and Technology for Sustainable Development in the South (COMSATS), Pakistan; Pontificia Universidad Católica del Perú, Peru; Ministry of Education and Science, National Science Centre and WUT ID-UB, Poland; Korea Institute of Science and Technology Information and National Research Foundation of Korea (NRF), Republic of Korea; Ministry of Education and Scientific Research, Institute of Atomic Physics and Ministry of Research and Innovation and Institute of Atomic Physics, Romania; Joint Institute for Nuclear Research (JINR), Ministry of Education and Science of the Russian Federation, National Research Centre Kurchatov Institute, Russian Science Foundation and Russian Foundation for Basic Research, Russia; Ministry of Education, Science, Research and Sport of the Slovak Republic, Slovakia; National Research Foundation of South Africa, South Africa; Swedish Research Council (VR) and Knut & Alice Wallenberg Foundation (KAW), Sweden; European Organization for Nuclear Research, Switzerland; Suranaree University of Technology (SUT), National Science and Technology Development Agency (NSDTA) and Office of the Higher Education Commission under NRU project of Thailand, Thailand; Turkish Energy, Nuclear and Mineral Research Agency (TENMAK), Turkey; National Academy of Sciences of Ukraine, Ukraine; Science and Technology Facilities Council (STFC), United Kingdom; National Science Foundation of the United States of America (NSF) and United States Department of Energy, Office of Nuclear Physics (DOE NP), United States of America.

References

[1] **STAR** Collaboration, J. Adams *et al.*, "Experimental and theoretical challenges in the search for the quark gluon plasma: The STAR Collaboration's critical assessment of the evidence from RHIC collisions," *Nucl. Phys. A* **757** (2005) 102–183, arXiv:nucl-ex/0501009.

[2] **PHENIX** Collaboration, K. Adcox *et al.*, "Formation of dense partonic matter in relativistic nucleus-nucleus collisions at RHIC: Experimental evaluation by the PHENIX collaboration," *Nucl. Phys. A* **757** (2005) 184–283, arXiv:nucl-ex/0410003.

[3] B. Müller, J. Schukraft, and B. Wysłouch, "First Results from Pb+Pb Collisions at the LHC," *Annu. Rev. Nucl. Part. S.* **62** (2012) 361–386.

[4] P. Braun-Munzinger, V. Koch, T. Schäfer, and J. Stachel, "Properties of hot and dense matter from relativistic heavy ion collisions," *Phys. Rept.* **621** (2016) 76–126.

[5] W. Busza, K. Rajagopal, and W. van der Schee, "Heavy Ion Collisions: The Big Picture, and the Big Questions," *Ann. Rev. Nucl. Part. Sci.* **68** (2018) 339–376.

[6] J. D. Bjorken, "Highly relativistic nucleus-nucleus collisions: The central rapidity region," *Phys. Rev. D* **27** (1983) 140–151.

[7] G.-Y. Qin and X.-N. Wang, "Jet quenching in high-energy heavy-ion collisions," *Int. J. Mod. Phys. E* **24** (2015) 1530014.

[8] J.-P. Blaizot and Y. Mehtar-Tani, "Jet structure in heavy ion collisions," *Int. J. Mod. Phys. E* **24** (2015) 1530012.

[9] A. Majumder and M. van Leeuwen, "The theory and phenomenology of perturbative QCD based jet quenching," *Prog. Part. Nucl. Phys.* **66** (2011) 41–92.

[10] **ALICE** Collaboration, "Measurements of inclusive jet spectra in pp and central Pb–Pb collisions at $\sqrt{s_{NN}} = 5.02$ TeV," *Phys. Rev. C* **101** (2020) 034911.

[11] **ATLAS** Collaboration, "Measurement of the nuclear modification factor for inclusive jets in Pb+Pb collisions at $\sqrt{s_{NN}} = 5.02$ TeV with the ATLAS detector," *Phys. Lett. B* **790** (2019) 108–128.

[12] **CMS** Collaboration, "Measurement of inclusive jet cross sections in pp and Pb–Pb collisions at $\sqrt{s_{NN}} = 2.76$ TeV," *Phys. Rev. C* **96** (2017) 015202.

[13] **STAR** Collaboration, J. Adam *et al.*, "Measurement of inclusive charged-particle jet production in Au+Au collisions at $\sqrt{s_{NN}}$=200 GeV," `arXiv:2006.00582 [nucl-ex]`.

[14] **ALICE** Collaboration, "Measurement of jet quenching with semi-inclusive hadron-jet distributions in central Pb–Pb collisions at $\sqrt{s_{NN}} = 2.76$ TeV," *J. High Energ. Phys.* **2015** (2015) 170.

[15] **STAR** Collaboration, "Measurements of jet quenching with semi-inclusive hadron+jet distributions in Au + Au collisions at $\sqrt{s_{NN}} = 200$ GeV," *Phys. Rev. C* **96** (2017) 024905.

[16] **ALICE** Collaboration, "Medium modification of the shape of small-radius jets in central Pb–Pb collisions at $\sqrt{s_{NN}} = 2.76$ TeV," *J. High Energ. Phys.* **2018** (2018) 139.

[17] **ATLAS** Collaboration, "Measurement of jet fragmentation in Pb–Pb and pp collisions at $\sqrt{s_{NN}} = 5.02$ TeV with the ATLAS detector," *Phys. Rev. C* **98** (2018) 024908.

[18] **CMS** Collaboration, "Modification of jet shapes in Pb–Pb collisions at $\sqrt{s_{NN}} = 2.76$ TeV," *Physics Letters B* **730** (2014) 243–263.

[19] A. J. Larkoski, S. Marzani, G. Soyez, and J. Thaler, "Soft Drop," *J. High Energ. Phys.* **05** (2014) 146.

[20] M. Dasgupta, A. Fregoso, S. Marzani, and G. P. Salam, "Towards an understanding of jet substructure," *J. High Energ. Phys.* **09** (2013) 029.

[21] A. J. Larkoski, S. Marzani, and J. Thaler, "Sudakov Safety in Perturbative QCD," *Phys. Rev.* **D91** (2015) 111501.

[22] **CMS** Collaboration, "Measurement of the Splitting Function in pp and Pb–Pb Collisions at $\sqrt{s_{\rm NN}} = 5.02$ TeV," *Phys. Rev. Lett.* **120** (2018) 142302.

[23] **ALICE** Collaboration, "Exploration of jet substructure using iterative declustering in pp and Pb–Pb collisions at LHC energies," *Phys. Lett. B* **802** (2020) 135227.

[24] **CMS** Collaboration, "Measurement of the groomed jet mass in Pb–Pb and pp collisions at $\sqrt{s_{\rm NN}} = 5.02$ TeV," *J. High Energ. Phys.* **2018** (2018) 161.

[25] Y. L. Dokshitzer, G. D. Leder, S. Moretti, and B. R. Webber, "Better jet clustering algorithms," *JHEP* **08** (1997) 001, arXiv:hep-ph/9707323.

[26] Z.-B. Kang, K. Lee, X. Liu, D. Neill, and F. Ringer, "The soft drop groomed jet radius at NLL," *J. High Energ. Phys.* **02** (2020) 054, arXiv:1908.01783 [hep-ph].

[27] **ATLAS** Collaboration, "Measurement of soft-drop jet observables in pp collisions with the ATLAS detector at $\sqrt{s_{\rm NN}} = 13$ TeV," *Phys. Rev. D* **101** (2020) 052007.

[28] **CMS** Collaboration, "Measurement of jet substructure observables in $t\bar{t}$ events from proton-proton collisions at $\sqrt{s} = 13$ TeV," *Phys. Rev. D* **98** (2018) 092014.

[29] A. Tripathee, W. Xue, A. Larkoski, S. Marzani, and J. Thaler, "Jet Substructure Studies with CMS Open Data," *Phys. Rev. D* **96** (2017) 074003.

[30] **STAR** Collaboration, J. Adam *et al.*, "Measurement of groomed jet substructure observables in p+p collisions at $\sqrt{s}$ =200 GeV with STAR," *Phys. Lett. B* **811** (2020) 135846, arXiv:2003.02114 [hep-ex].

[31] F. Ringer, B.-W. Xiao, and F. Yuan, "Can we observe jet P_T-broadening in heavy-ion collisions at the LHC?," *Phys. Lett. B* **808** (2020) 135634, arXiv:1907.12541 [hep-ph].

[32] J. Casalderrey-Solana, Y. Mehtar-Tani, C. A. Salgado, and K. Tywoniuk, "New picture of jet quenching dictated by color coherence," *Phys. Lett. B* **725** (2013) 357–360.

[33] Y.-T. Chien and I. Vitev, "Probing the Hardest Branching within Jets in Heavy-Ion Collisions," *Phys. Rev. Lett.* **119** (2017) 112301.

[34] P. Caucal, E. Iancu, and G. Soyez, "Deciphering the z_g distribution in ultrarelativistic heavy ion collisions," *J. High Energ. Phys.* **10** (2019) 273.

[35] N.-B. Chang, S. Cao, and G.-Y. Qin, "Probing medium-induced jet splitting and energy loss in heavy-ion collisions," *Physics Letters B* **781** (2018) 423–432.

[36] J. Casalderrey-Solana, G. Milhano, D. Pablos, and K. Rajagopal, "Modification of Jet Substructure in Heavy Ion Collisions as a Probe of the Resolution Length of Quark-Gluon Plasma," *J. High Energ. Phys.* **01** (2020) 044.

[37] J. Mulligan and M. Ploskon, "Identifying groomed jet splittings in heavy-ion collisions," *Phys. Rev. C* **102** (2020) 044913, arXiv:2006.01812 [hep-ph].

[38] **ALICE** Collaboration, K. Aamodt *et al.*, "The ALICE experiment at the CERN LHC," *JINST* **3** (2008) S08002.

[39] **ALICE** Collaboration, "Performance of the ALICE Experiment at the CERN LHC," *Int. J. Mod. Phys. A* **29** (2014) 1430044.

[40] **ALICE** Collaboration, "Performance of the ALICE VZERO system," *JINST* **8** (2013) P10016.

[41] **ALICE** Collaboration, "Centrality determination of Pb–Pb collisions at $\sqrt{s_{NN}} = 2.76$ TeV with ALICE," *Phys. Rev. C* **88** (2013) 044909.

[42] **ALICE** Collaboration, "Centrality determination in heavy-ion collisions." http://cds.cern.ch/record/2636623.

[43] **ALICE** Collaboration, "ALICE 2017 luminosity determination for pp collisions at $\sqrt{s}$ =5 TeV,". http://cds.cern.ch/record/2648933.

[44] J. Alme and et al., "The ALICE TPC, a large 3-dimensional tracking device with fast readout for ultra-high multiplicity events," *Nucl. Instrum. Meth. A: Accelerators, Spectrometers, Detectors and Associated Equipment* **622** (2010) 316–367.

[45] **ALICE** Collaboration, "Alignment of the ALICE Inner Tracking System with cosmic-ray tracks," *JINST* **5** (2010) P03003.

[46] R. Brun, F. Bruyant, M. Maire, A. C. McPherson, and P. Zanarini, *GEANT 3: user's guide Geant 3.10, Geant 3.11; rev. version*. CERN, Geneva, 1987. https://cds.cern.ch/record/1119728.

[47] T. Sjostrand, S. Ask, J. R. Christiansen, R. Corke, N. Desai, P. Ilten, S. Mrenna, S. Prestel, C. O. Rasmussen, and P. Z. Skands, "An introduction to PYTHIA 8.2," *Comput. Phys. Commun.* **191** (2015) 159–177.

[48] M. Gyulassy and X.-N. Wang, "Hijing 1.0: A monte carlo program for parton and particle production in high energy hadronic and nuclear collisions," *Comput. Phys. Commun.* **83** (1994) 307 – 331.

[49] M. Cacciari, G. P. Salam, and G. Soyez, "FastJet User Manual," *Eur. Phys. J. C* **72** (2012) 1896.

[50] M. Cacciari, G. P. Salam, and G. Soyez, "The anti-k_t jet clustering algorithm," *J. High Energ. Phys.* **04** (2008) 063.

[51] M. Cacciari, G. P. Salam, and G. Soyez, "The Catchment Area of Jets," *J. High Energ. Phys.* **04** (2008) 005.

[52] P. Berta, M. Spousta, D. W. Miller, and R. Leitner, "Particle-level pileup subtraction for jets and jet shapes," *J. High Energ. Phys.* **06** (2014) 092.

[53] P. Berta, L. Masetti, D. Miller, and M. Spousta, "Pileup and Underlying Event Mitigation with Iterative Constituent Subtraction," *J. High Energ. Phys.* **08** (2019) 175.

[54] G. D'Agostini, "A multidimensional unfolding method based on bayes' theorem," *Nucl. Instrum. Meth. A: Accelerators, Spectrometers, Detectors and Associated Equipment* **362** (1995) 487 – 498.

[55] "RooUnfold." http://hepunx.rl.ac.uk/~adye/software/unfold/RooUnfold.html. Access date: May 31 2020.

[56] **ALICE** Collaboration, "Measurement of event background fluctuations for charged particle jet reconstruction in Pb–Pb collisions at $\sqrt{s_{NN}} = 2.76$ TeV," *J. High Energ. Phys.* **2012** (2012) 53.

[57] J. Bellm *et al.*, "Herwig 7.0/Herwig++ 3.0 release note," *Eur. Phys. J. C* **76** no. 4, (Apr, 2016) 196, arXiv:1512.01178 [hep-ph].

[58] K. C. Zapp, "JEWEL 2.0.0: directions for use," *Eur. Phys. J. C* **74** no. 2, (2014) 2762, arXiv:1311.0048 [hep-ph].

[59] R. Kunnawalkam Elayavalli and K. C. Zapp, "Medium response in JEWEL and its impact on jet shape observables in heavy ion collisions," *JHEP* **07** (2017) 141, arXiv:1707.01539 [hep-ph].

[60] **JETSCAPE** Collaboration, J. Putschke *et al.*, "The JETSCAPE framework," arXiv:1903.07706 [nucl-th].

[61] P. Caucal, E. Iancu, A. H. Mueller, and G. Soyez, "Vacuum-like jet fragmentation in a dense QCD medium," *Phys. Rev. Lett.* **120** (2018) 232001, arXiv:1801.09703 [hep-ph].

[62] J. Casalderrey-Solana, D. C. Gulhan, J. G. Milhano, D. Pablos, and K. Rajagopal, "A Hybrid Strong/Weak Coupling Approach to Jet Quenching," *J. High Energ. Phys.* **10** (2014) 019, arXiv:1405.3864 [hep-ph]. [Erratum: *JHEP* **09** (2015), 175].

[63] Z. Hulcher, D. Pablos, and K. Rajagopal, "Resolution Effects in the Hybrid Strong/Weak Coupling Model," *J. High Energ. Phys.* **03** (2018) 010, arXiv:1707.05245 [hep-ph].

[64] A. Majumder, "Incorporating Space-Time Within Medium-Modified Jet Event Generators," *Phys. Rev. C* **88** (2013) 014909, arXiv:1301.5323 [nucl-th].

[65] Y. He, T. Luo, X.-N. Wang, and Y. Zhu, "Linear Boltzmann Transport for Jet Propagation in the Quark-Gluon Plasma: Elastic Processes and Medium Recoil," *Phys. Rev. C* **91** (2015) 054908, arXiv:1503.03313 [nucl-th]. [Erratum: *Phys.Rev.C* **97** (2018), 019902].

[66] K. C. Zapp, F. Krauss, and U. A. Wiedemann, "A perturbative framework for jet quenching," *J. High Energ. Phys.* **03** (2013) 080, arXiv:1212.1599 [hep-ph].

[67] J.-W. Qiu, F. Ringer, N. Sato, and P. Zurita, "Factorization of jet cross sections in heavy-ion collisions," *Phys. Rev. Lett.* **122** (2019) 252301.

[68] **CMS** Collaboration, "Measurement of quark- and gluon-like jet fractions using jet charge in PbPb and pp collisions at 5.02 TeV," *J. High Energ. Phys.* **07** (2020) 115.

A The ALICE Collaboration

S. Acharya[143], D. Adamová[98], A. Adler[76], G. Aglieri Rinella[35], M. Agnello[31], N. Agrawal[55], Z. Ahammed[143], S. Ahmad[16], S.U. Ahn[78], I. Ahuja[39], Z. Akbar[52], A. Akindinov[95], M. Al-Turany[110], S.N. Alam[16,41], D. Aleksandrov[91], B. Alessandro[61], H.M. Alfanda[7], R. Alfaro Molina[73], B. Ali[16], Y. Ali[14], A. Alici[26], N. Alizadehvandchali[127], A. Alkin[35], J. Alme[21], T. Alt[70], L. Altenkamper[21], I. Altsybeev[115], M.N. Anaam[7], C. Andrei[49], D. Andreou[93], A. Andronic[146], M. Angeletti[35], V. Anguelov[107], F. Antinori[58], P. Antonioli[55], C. Anuj[16], N. Apadula[82], L. Aphecetche[117], H. Appelshäuser[70], S. Arcelli[26], R. Arnaldi[61], I.C. Arsene[20], M. Arslandok[148,107], A. Augustinus[35], R. Averbeck[110], S. Aziz[80], M.D. Azmi[16], A. Badalà[57], Y.W. Baek[42], X. Bai[131,110], R. Bailhache[70], Y. Bailung[51], R. Bala[104], A. Balbino[31], A. Baldisseri[140], B. Balis[2], M. Ball[44], D. Banerjee[4], R. Barbera[27], L. Barioglio[108], M. Barlou[87], G.G. Barnaföldi[147], L.S. Barnby[97], V. Barret[137], C. Bartels[130], K. Barth[35], E. Bartsch[70], F. Baruffaldi[28], N. Bastid[137], S. Basu[83], G. Batigne[117], B. Batyunya[77], D. Bauri[50], J.L. Bazo Alba[114], I.G. Bearden[92], C. Beattie[148], I. Belikov[139], A.D.C. Bell Hechavarria[146], F. Bellini[26], R. Bellwied[127], S. Belokurova[115], V. Belyaev[96], G. Bencedi[71], S. Beole[25], A. Bercuci[49], Y. Berdnikov[101], A. Berdnikova[107], L. Bergmann[107], M.G. Besoiu[69], L. Betev[35], P.P. Bhaduri[143], A. Bhasin[104], I.R. Bhat[104], M.A. Bhat[4], B. Bhattacharjee[43], P. Bhattacharya[23], L. Bianchi[25], N. Bianchi[53], J. Bielčík[38], J. Bielčíková[98], J. Biernat[120], A. Bilandzic[108], G. Biro[147], S. Biswas[4], J.T. Blair[121], D. Blau[91,84], M.B. Blidaru[110], C. Blume[70], G. Boca[29,59], F. Bock[99], A. Bogdanov[96], S. Boi[23], J. Bok[63], L. Boldizsár[147], A. Bolozdynya[96], M. Bombara[39], P.M. Bond[35], G. Bonomi[142,59], H. Borel[140], A. Borissov[84], H. Bossi[148], E. Botta[25], L. Bratrud[70], P. Braun-Munzinger[110], M. Bregant[123], M. Broz[38], G.E. Bruno[109,34], M.D. Buckland[130], D. Budnikov[111], H. Buesching[70], S. Bufalino[31], O. Bugnon[117], P. Buhler[116], Z. Buthelezi[74,134], J.B. Butt[14], S.A. Bysiak[120], M. Cai[28,7], H. Caines[148], A. Caliva[110], E. Calvo Villar[114], J.M.M. Camacho[122], R.S. Camacho[46], P. Camerini[24], F.D.M. Canedo[123], F. Carnesecchi[35,26], R. Caron[140], J. Castillo Castellanos[140], E.A.R. Casula[23], F. Catalano[31], C. Ceballos Sanchez[77], P. Chakraborty[50], S. Chandra[143], S. Chapeland[35], M. Chartier[130], S. Chattopadhyay[143], S. Chattopadhyay[112], A. Chauvin[23], T.G. Chavez[46], T. Cheng[7], C. Cheshkov[138], B. Cheynis[138], V. Chibante Barroso[35], D.D. Chinellato[124], S. Cho[63], P. Chochula[35], P. Christakoglou[93], C.H. Christensen[92], P. Christiansen[83], T. Chujo[136], C. Cicalo[56], L. Cifarelli[26], F. Cindolo[55], M.R. Ciupek[110], G. Clai[II,55], J. Cleymans[I,126], F. Colamaria[54], J.S. Colburn[113], D. Colella[109,54,34,147], A. Collu[82], M. Colocci[35], M. Concas[III,61], G. Conesa Balbastre[81], Z. Conesa del Valle[80], G. Contin[24], J.G. Contreras[38], M.L. Coquet[140], T.M. Cormier[99], P. Cortese[32], M.R. Cosentino[125], F. Costa[35], S. Costanza[29,59], P. Crochet[137], R. Cruz-Torres[82], E. Cuautle[71], P. Cui[7], L. Cunqueiro[99], A. Dainese[58], M.C. Danisch[107], A. Danu[69], I. Das[112], P. Das[89], P. Das[4], S. Das[4], S. Dash[50], S. De[89], A. De Caro[30], G. de Cataldo[54], L. De Cilladi[25], J. de Cuveland[40], A. De Falco[23], D. De Gruttola[30], N. De Marco[61], C. De Martin[24], S. De Pasquale[30], S. Deb[51], H.F. Degenhardt[123], K.R. Deja[144], L. Dello Stritto[30], S. Delsanto[25], W. Deng[7], P. Dhankher[19], D. Di Bari[34], A. Di Mauro[35], R.A. Diaz[8], T. Dietel[126], Y. Ding[138,7], R. Divià[35], D.U. Dixit[19], Ø. Djuvsland[21], U. Dmitrieva[65], J. Do[63], A. Dobrin[69], B. Dönigus[70], O. Dordic[20], A.K. Dubey[143], A. Dubla[110,93], S. Dudi[103], M. Dukhishyam[89], P. Dupieux[137], N. Dzalaiova[13], T.M. Eder[146], R.J. Ehlers[99], V.N. Eikeland[21], F. Eisenhut[70], D. Elia[54], B. Erazmus[117], F. Ercolessi[26], F. Erhardt[102], A. Erokhin[115], M.R. Ersdal[21], B. Espagnon[80], G. Eulisse[35], D. Evans[113], S. Evdokimov[94], L. Fabbietti[108], M. Faggin[28], J. Faivre[81], F. Fan[7], A. Fantoni[53], M. Fasel[99], P. Fecchio[31], A. Feliciello[61], G. Feofilov[115], A. Fernández Téllez[46], A. Ferrero[140], A. Ferretti[25], V.J.G. Feuillard[107], J. Figiel[120], S. Filchagin[111], D. Finogeev[65], F.M. Fionda[56,21], G. Fiorenza[35,109], F. Flor[127], A.N. Flores[121], S. Foertsch[74], P. Foka[110], S. Fokin[91], E. Fragiacomo[62], E. Frajna[147], U. Fuchs[35], N. Funicello[30], C. Furget[81], A. Furs[65], J.J. Gaardhøje[92], M. Gagliardi[25], A.M. Gago[114], A. Gal[139], C.D. Galvan[122], P. Ganoti[87], C. Garabatos[110], J.R.A. Garcia[46], E. Garcia-Solis[10], K. Garg[117], C. Gargiulo[35], A. Garibli[90], K. Garner[146], P. Gasik[110], E.F. Gauger[121], A. Gautam[129], M.B. Gay Ducati[72], M. Germain[117], P. Ghosh[143], S.K. Ghosh[4], M. Giacalone[26], P. Gianotti[53], P. Giubellino[110,61], P. Giubilato[28], A.M.C. Glaenzer[140], P. Glässel[107], D.J.Q. Goh[85], V. Gonzalez[145], L.H. González-Trueba[73], S. Gorbunov[40], M. Gorgon[2], L. Görlich[120], S. Gotovac[36], V. Grabski[73], L.K. Graczykowski[144], L. Greiner[82], A. Grelli[64], C. Grigoras[35], V. Grigoriev[96], S. Grigoryan[77,1], O.S. Groettvik[21], F. Grosa[35,61], J.F. Grosse-Oetringhaus[35], R. Grosso[110], G.G. Guardiano[124], R. Guernane[81], M. Guilbaud[117], K. Gulbrandsen[92], T. Gunji[135], W. Guo[7], A. Gupta[104], R. Gupta[104], S.P. Guzman[46], L. Gyulai[147], M.K. Habib[110], C. Hadjidakis[80], G. Halimoglu[70], H. Hamagaki[85], G. Hamar[147], M. Hamid[7], R. Hannigan[121], M.R. Haque[144,89], A. Harlenderova[110], J.W. Harris[148], A. Harton[10], J.A. Hasenbichler[35], H. Hassan[99], D. Hatzifotiadou[55], P. Hauer[44], L.B. Havener[148], S. Hayashi[135], S.T. Heckel[108], E. Hellbär[110], H. Helstrup[37], T. Herman[38], E.G. Hernandez[46], G. Herrera Corral[9], F. Herrmann[146], K.F. Hetland[37], H. Hillemanns[35], C. Hills[130], B. Hippolyte[139], B. Hofman[64], B. Hohlweger[93], J. Honermann[146], G.H. Hong[149], D. Horak[38], S. Hornung[110], A. Horzyk[2], R. Hosokawa[15], Y. Hou[7], P. Hristov[35], C. Hughes[133], P. Huhn[70], T.J. Humanic[100], H. Hushnud[112], L.A. Husova[146], A. Hutson[127], D. Hutter[40], J.P. Iddon[35,130], R. Ilkaev[111], H. Ilyas[14], M. Inaba[136],

G.M. Innocenti[35], M. Ippolitov[91], A. Isakov[38,98], M.S. Islam[112], M. Ivanov[110], V. Ivanov[101], V. Izucheev[94], M. Jablonski[2], B. Jacak[82], N. Jacazio[35], P.M. Jacobs[82], S. Jadlovska[119], J. Jadlovsky[119], S. Jaelani[64], C. Jahnke[124,123], M.J. Jakubowska[144], A. Jalotra[104], M.A. Janik[144], T. Janson[76], M. Jercic[102], O. Jevons[113], A.A.P. Jimenez[71], F. Jonas[99,146], P.G. Jones[113], J.M. Jowett [35,110], J. Jung[70], M. Jung[70], A. Junique[35], A. Jusko[113], J. Kaewjai[118], P. Kalinak[66], A. Kalweit[35], V. Kaplin[96], S. Kar[7], A. Karasu Uysal[79], D. Karatovic[102], O. Karavichev[65], T. Karavicheva[65], P. Karczmarczyk[144], E. Karpechev[65], A. Kazantsev[91], U. Kebschull[76], R. Keidel[48], D.L.D. Keijdener[64], M. Keil[35], B. Ketzer[44], Z. Khabanova[93], A.M. Khan[7], S. Khan[16], A. Khanzadeev[101], Y. Kharlov[94,84], A. Khatun[16], A. Khuntia[120], B. Kileng[37], B. Kim[17,63], C. Kim[17], D.J. Kim[128], E.J. Kim[75], J. Kim[149], J.S. Kim[42], J. Kim[107], J. Kim[149], J. Kim[75], M. Kim[107], S. Kim[18], T. Kim[149], S. Kirsch[70], I. Kisel[40], S. Kiselev[95], A. Kisiel[144], J.P. Kitowski[2], J.L. Klay[6], J. Klein[35], S. Klein[82], C. Klein-Bösing[146], M. Kleiner[70], T. Klemenz[108], A. Kluge[35], A.G. Knospe[127], C. Kobdaj[118], M.K. Köhler[107], T. Kollegger[110], A. Kondratyev[77], N. Kondratyeva[96], E. Kondratyuk[94], J. Konig[70], S.A. Konigstorfer[108], P.J. Konopka[35,2], G. Kornakov[144], S.D. Koryciak[2], L. Koska[119], A. Kotliarov[98], O. Kovalenko[88], V. Kovalenko[115], M. Kowalski[120], I. Králik[66], A. Kravčáková[39], L. Kreis[110], M. Krivda[113,66], F. Krizek[98], K. Krizkova Gajdosova[38], M. Kroesen[107], M. Krüger[70], E. Kryshen[101], M. Krzewicki[40], V. Kučera[35], C. Kuhn[139], P.G. Kuijer[93], T. Kumaoka[136], D. Kumar[143], L. Kumar[103], N. Kumar[103], S. Kundu[35,89], P. Kurashvili[88], A. Kurepin[65], A.B. Kurepin[65], A. Kuryakin[111], S. Kushpil[98], J. Kvapil[113], M.J. Kweon[63], J.Y. Kwon[63], Y. Kwon[149], S.L. La Pointe[40], P. La Rocca[27], Y.S. Lai[82], A. Lakrathok[118], M. Lamanna[35], R. Langoy[132], K. Lapidus[35], P. Larionov[35,53], E. Laudi[35], L. Lautner[35,108], R. Lavicka[38], T. Lazareva[115], R. Lea[142,24,59], J. Lehrbach[40], R.C. Lemmon[97], I. León Monzón[122], E.D. Lesser[19], M. Lettrich[35,108], P. Lévai[147], X. Li[11], X.L. Li[7], J. Lien[132], R. Lietava[113], B. Lim[17], S.H. Lim[17], V. Lindenstruth[40], A. Lindner[49], C. Lippmann[110], A. Liu[19], D.H. Liu[7], J. Liu[130], I.M. Lofnes[21], V. Loginov[96], C. Loizides[99], P. Loncar[36], J.A. Lopez[107], X. Lopez[137], E. López Torres[8], J.R. Luhder[146], M. Lunardon[28], G. Luparello[62], Y.G. Ma[41], A. Maevskaya[65], M. Mager[35], T. Mahmoud[44], A. Maire[139], M. Malaev[101], N.M. Malik[104], Q.W. Malik[20], L. Malinina[IV,77], D. Mal'Kevich[95], N. Mallick[51], P. Malzacher[110], G. Mandaglio[33,57], V. Manko[91], F. Manso[137], V. Manzari[54], Y. Mao[7], J. Mareš[68], G.V. Margagliotti[24], A. Margotti[55], A. Marín[110], C. Markert[121], M. Marquard[70], N.A. Martin[107], P. Martinengo[35], J.L. Martinez[127], M.I. Martínez[46], G. Martínez García[117], S. Masciocchi[110], M. Masera[25], A. Masoni[56], L. Massacrier[80], A. Mastroserio[141,54], A.M. Mathis[108], O. Matonoha[83], P.F.T. Matuoka[123], A. Matyja[120], C. Mayer[120], A.L. Mazuecos[35], F. Mazzaschi[25], M. Mazzilli[35], M.A. Mazzoni[I,60], J.E. Mdhluli[134], A.F. Mechler[70], F. Meddi[22], Y. Melikyan[65], A. Menchaca-Rocha[73], E. Meninno[116,30], A.S. Menon[127], M. Meres[13], S. Mhlanga[126,74], Y. Miake[136], L. Micheletti[61,25], L.C. Migliorin[138], D.L. Mihaylov[108], K. Mikhaylov[77,95], A.N. Mishra[147], D. Miśkowiec[110], A. Modak[4], A.P. Mohanty[64], B. Mohanty[89], M. Mohisin Khan[V,16], M.A. Molander[45], Z. Moravcova[92], C. Mordasini[108], D.A. Moreira De Godoy[146], L.A.P. Moreno[46], I. Morozov[65], A. Morsch[35], T. Mrnjavac[35], V. Muccifora[53], E. Mudnic[36], D. Mühlheim[146], S. Muhuri[143], J.D. Mulligan[82], A. Mulliri[23], M.G. Munhoz[123], R.H. Munzer[70], H. Murakami[135], S. Murray[126], L. Musa[35], J. Musinsky[66], J.W. Myrcha[144], B. Naik[134,50], R. Nair[88], B.K. Nandi[50], R. Nania[55], E. Nappi[54], A.F. Nassirpour[83], A. Nath[107], C. Nattrass[133], A. Neagu[20], L. Nellen[71], S.V. Nesbo[37], G. Neskovic[40], D. Nesterov[115], B.S. Nielsen[92], S. Nikolaev[91], S. Nikulin[91], V. Nikulin[101], F. Noferini[55], S. Noh[12], P. Nomokonov[77], J. Norman[130], N. Novitzky[136], P. Nowakowski[144], A. Nyanin[91], J. Nystrand[21], M. Ogino[85], A. Ohlson[83], V.A. Okorokov[96], J. Oleniacz[144], A.C. Oliveira Da Silva[133], M.H. Oliver[148], A. Onnerstad[128], C. Oppedisano[61], A. Ortiz Velasquez[71], T. Osako[47], A. Oskarsson[83], J. Otwinowski[120], M. Oya[47], K. Oyama[85], Y. Pachmayer[107], S. Padhan[50], D. Pagano[142,59], G. Paić[71], A. Palasciano[54], J. Pan[145], S. Panebianco[140], P. Pareek[143], J. Park[63], J.E. Parkkila[128], S.P. Pathak[127], R.N. Patra[104,35], B. Paul[23], H. Pei[7], T. Peitzmann[64], X. Peng[7], L.G. Pereira[72], H. Pereira Da Costa[140], D. Peresunko[91,84], G.M. Perez[8], S. Perrin[140], Y. Pestov[5], V. Petráček[38], M. Petrovici[49], R.P. Pezzi[117,72], S. Piano[62], M. Pikna[13], P. Pillot[117], O. Pinazza[55,35], L. Pinsky[127], C. Pinto[27], S. Pisano[53], M. Płoskoń[82], M. Planinic[102], F. Pliquett[70], M.G. Poghosyan[99], B. Polichtchouk[94], S. Politano[31], N. Poljak[102], A. Pop[49], S. Porteboeuf-Houssais[137], J. Porter[82], V. Pozdniakov[77], S.K. Prasad[4], R. Preghenella[55], F. Prino[61], C.A. Pruneau[145], I. Pshenichnov[65], M. Puccio[35], S. Qiu[93], L. Quaglia[25], R.E. Quishpe[127], S. Ragoni[113], A. Rakotozafindrabe[140], L. Ramello[32], F. Rami[139], S.A.R. Ramirez[46], A.G.T. Ramos[34], T.A. Rancien[81], R. Raniwala[105], S. Raniwala[105], S.S. Räsänen[45], R. Rath[51], I. Ravasenga[93], K.F. Read[99,133], A.R. Redelbach[40], K. Redlich[VI,88], A. Rehman[21], P. Reichelt[70], F. Reidt[35], H.A. Reme-ness[37], R. Renfordt[70], Z. Rescakova[39], K. Reygers[107], A. Riabov[101], V. Riabov[101], T. Richert[83], M. Richter[20], W. Riegler[35], F. Riggi[27], C. Ristea[69], M. Rodríguez Cahuantzi[46], K. Røed[20], R. Rogalev[94], E. Rogochaya[77], T.S. Rogoschinski[70], D. Rohr[35], D. Röhrich[21], P.F. Rojas[46], P.S. Rokita[144], F. Ronchetti[53], A. Rosano[33,57], E.D. Rosas[71], A. Rossi[58], A. Rotondi[29,59], A. Roy[51], P. Roy[112], S. Roy[50], N. Rubini[26], O.V. Rueda[83], R. Rui[24], B. Rumyantsev[77], P.G. Russek[2], A. Rustamov[90], E. Ryabinkin[91], Y. Ryabov[101], A. Rybicki[120], H. Rytkonen[128], W. Rzesa[144],

O.A.M. Saarimaki[45], R. Sadek[117], S. Sadovsky[94], J. Saetre[21], K. Šafařík[38], S.K. Saha[143], S. Saha[89], B. Sahoo[50], P. Sahoo[50], R. Sahoo[51], S. Sahoo[67], D. Sahu[51], P.K. Sahu[67], J. Saini[143], S. Sakai[136], S. Sambyal[104], V. Samsonov[I,101,96], D. Sarkar[145], N. Sarkar[143], P. Sarma[43], V.M. Sarti[108], M.H.P. Sas[148], J. Schambach[99,121], H.S. Scheid[70], C. Schiaua[49], R. Schicker[107], A. Schmah[107], C. Schmidt[110], H.R. Schmidt[106], M.O. Schmidt[35], M. Schmidt[106], N.V. Schmidt[99,70], A.R. Schmier[133], R. Schotter[139], J. Schukraft[35], Y. Schutz[139], K. Schwarz[110], K. Schweda[110], G. Scioli[26], E. Scomparin[61], J.E. Seger[15], Y. Sekiguchi[135], D. Sekihata[135], I. Selyuzhenkov[110,96], S. Senyukov[139], J.J. Seo[63], D. Serebryakov[65], L. Šerkšnytė[108], A. Sevcenco[69], T.J. Shaba[74], A. Shabanov[65], A. Shabetai[117], R. Shahoyan[35], W. Shaikh[112], A. Shangaraev[94], A. Sharma[103], H. Sharma[120], M. Sharma[104], N. Sharma[103], S. Sharma[104], U. Sharma[104], O. Sheibani[127], K. Shigaki[47], M. Shimomura[86], S. Shirinkin[95], Q. Shou[41], Y. Sibiriak[91], S. Siddhanta[56], T. Siemiarczuk[88], T.F. Silva[123], D. Silvermyr[83], G. Simonetti[35], B. Singh[108], R. Singh[89], R. Singh[104], R. Singh[51], V.K. Singh[143], V. Singhal[143], T. Sinha[112], B. Sitar[13], M. Sitta[32], T.B. Skaali[20], G. Skorodumovs[107], M. Slupecki[45], N. Smirnov[148], R.J.M. Snellings[64], C. Soncco[114], J. Song[127], A. Songmoolnak[118], F. Soramel[28], S. Sorensen[133], I. Sputowska[120], J. Stachel[107], I. Stan[69], P.J. Steffanic[133], S.F. Stiefelmaier[107], D. Stocco[117], I. Storehaug[20], M.M. Storetvedt[37], C.P. Stylianidis[93], A.A.P. Suaide[123], T. Sugitate[47], C. Suire[80], M. Sukhanov[65], M. Suljic[35], R. Sultanov[95], M. Šumbera[98], V. Sumberia[104], S. Sumowidagdo[52], S. Swain[67], A. Szabo[13], I. Szarka[13], U. Tabassam[14], S.F. Taghavi[108], G. Taillepied[137], J. Takahashi[124], G.J. Tambave[21], S. Tang[137,7], Z. Tang[131], J.D. Tapia Takaki[VII,129], M. Tarhini[117], M.G. Tarzila[49], A. Tauro[35], G. Tejeda Muñoz[46], A. Telesca[35], L. Terlizzi[25], C. Terrevoli[127], G. Tersimonov[3], S. Thakur[143], D. Thomas[121], R. Tieulent[138], A. Tikhonov[65], A.R. Timmins[127], M. Tkacik[119], A. Toia[70], N. Topilskaya[65], M. Toppi[53], F. Torales-Acosta[19], T. Tork[80], S.R. Torres[38], A. Trifiró[33,57], S. Tripathy[55,71], T. Tripathy[50], S. Trogolo[35,28], G. Trombetta[34], V. Trubnikov[3], W.H. Trzaska[128], T.P. Trzcinski[144], B.A. Trzeciak[38], A. Tumkin[111], R. Turrisi[58], T.S. Tveter[20], K. Ullaland[21], A. Uras[138], M. Urioni[59,142], G.L. Usai[23], M. Vala[39], N. Valle[59,29], S. Vallero[61], N. van der Kolk[64], L.V.R. van Doremalen[64], M. van Leeuwen[93], P. Vande Vyvre[35], D. Varga[147], Z. Varga[147], M. Varga-Kofarago[147], A. Vargas[46], M. Vasileiou[87], A. Vasiliev[91], O. Vázquez Doce[53,108], V. Vechernin[115], E. Vercellin[25], S. Vergara Limón[46], L. Vermunt[64], R. Vértesi[147], M. Verweij[64], L. Vickovic[36], Z. Vilakazi[134], O. Villalobos Baillie[113], G. Vino[54], A. Vinogradov[91], T. Virgili[30], V. Vislavicius[92], A. Vodopyanov[77], B. Volkel[35], M.A. Völkl[107], K. Voloshin[95], S.A. Voloshin[145], G. Volpe[34], B. von Haller[35], I. Vorobyev[108], D. Voscek[119], N. Vozniuk[65], J. Vrláková[39], B. Wagner[21], C. Wang[41], D. Wang[41], M. Weber[116], R.J.G.V. Weelden[93], A. Wegrzynek[35], S.C. Wenzel[35], J.P. Wessels[146], J. Wiechula[70], J. Wikne[20], G. Wilk[88], J. Wilkinson[110], G.A. Willems[146], B. Windelband[107], M. Winn[140], W.E. Witt[133], J.R. Wright[121], W. Wu[41], Y. Wu[131], R. Xu[7], A.K. Yadav[143], S. Yalcin[79], Y. Yamaguchi[47], K. Yamakawa[47], S. Yang[21], S. Yano[47], Z. Yin[7], H. Yokoyama[64], I.-K. Yoo[17], J.H. Yoon[63], S. Yuan[21], A. Yuncu[107], V. Zaccolo[24], C. Zampolli[35], H.J.C. Zanoli[64], N. Zardoshti[35], A. Zarochentsev[115], P. Závada[68], N. Zaviyalov[111], M. Zhalov[101], B. Zhang[7], S. Zhang[41], X. Zhang[7], Y. Zhang[131], V. Zherebchevskii[115], Y. Zhi[11], N. Zhigareva[95], D. Zhou[7], Y. Zhou[92], J. Zhu[7,110], Y. Zhu[7], A. Zichichi[26], G. Zinovjev[3], N. Zurlo[142,59]

Affiliation notes

[I] Deceased
[II] Also at: Italian National Agency for New Technologies, Energy and Sustainable Economic Development (ENEA), Bologna, Italy
[III] Also at: Dipartimento DET del Politecnico di Torino, Turin, Italy
[IV] Also at: M.V. Lomonosov Moscow State University, D.V. Skobeltsyn Institute of Nuclear, Physics, Moscow, Russia
[V] Also at: Department of Applied Physics, Aligarh Muslim University, Aligarh, India
[VI] Also at: Institute of Theoretical Physics, University of Wroclaw, Poland
[VII] Also at: University of Kansas, Lawrence, Kansas, United States

Collaboration Institutes

[1] A.I. Alikhanyan National Science Laboratory (Yerevan Physics Institute) Foundation, Yerevan, Armenia
[2] AGH University of Science and Technology, Cracow, Poland
[3] Bogolyubov Institute for Theoretical Physics, National Academy of Sciences of Ukraine, Kiev, Ukraine
[4] Bose Institute, Department of Physics and Centre for Astroparticle Physics and Space Science (CAPSS), Kolkata, India
[5] Budker Institute for Nuclear Physics, Novosibirsk, Russia

[6] California Polytechnic State University, San Luis Obispo, California, United States
[7] Central China Normal University, Wuhan, China
[8] Centro de Aplicaciones Tecnológicas y Desarrollo Nuclear (CEADEN), Havana, Cuba
[9] Centro de Investigación y de Estudios Avanzados (CINVESTAV), Mexico City and Mérida, Mexico
[10] Chicago State University, Chicago, Illinois, United States
[11] China Institute of Atomic Energy, Beijing, China
[12] Chungbuk National University, Cheongju, Republic of Korea
[13] Comenius University Bratislava, Faculty of Mathematics, Physics and Informatics, Bratislava, Slovakia
[14] COMSATS University Islamabad, Islamabad, Pakistan
[15] Creighton University, Omaha, Nebraska, United States
[16] Department of Physics, Aligarh Muslim University, Aligarh, India
[17] Department of Physics, Pusan National University, Pusan, Republic of Korea
[18] Department of Physics, Sejong University, Seoul, Republic of Korea
[19] Department of Physics, University of California, Berkeley, California, United States
[20] Department of Physics, University of Oslo, Oslo, Norway
[21] Department of Physics and Technology, University of Bergen, Bergen, Norway
[22] Dipartimento di Fisica dell'Università 'La Sapienza' and Sezione INFN, Rome, Italy
[23] Dipartimento di Fisica dell'Università and Sezione INFN, Cagliari, Italy
[24] Dipartimento di Fisica dell'Università and Sezione INFN, Trieste, Italy
[25] Dipartimento di Fisica dell'Università and Sezione INFN, Turin, Italy
[26] Dipartimento di Fisica e Astronomia dell'Università and Sezione INFN, Bologna, Italy
[27] Dipartimento di Fisica e Astronomia dell'Università and Sezione INFN, Catania, Italy
[28] Dipartimento di Fisica e Astronomia dell'Università and Sezione INFN, Padova, Italy
[29] Dipartimento di Fisica e Nucleare e Teorica, Università di Pavia, Pavia, Italy
[30] Dipartimento di Fisica 'E.R. Caianiello' dell'Università and Gruppo Collegato INFN, Salerno, Italy
[31] Dipartimento DISAT del Politecnico and Sezione INFN, Turin, Italy
[32] Dipartimento di Scienze e Innovazione Tecnologica dell'Università del Piemonte Orientale and INFN Sezione di Torino, Alessandria, Italy
[33] Dipartimento di Scienze MIFT, Università di Messina, Messina, Italy
[34] Dipartimento Interateneo di Fisica 'M. Merlin' and Sezione INFN, Bari, Italy
[35] European Organization for Nuclear Research (CERN), Geneva, Switzerland
[36] Faculty of Electrical Engineering, Mechanical Engineering and Naval Architecture, University of Split, Split, Croatia
[37] Faculty of Engineering and Science, Western Norway University of Applied Sciences, Bergen, Norway
[38] Faculty of Nuclear Sciences and Physical Engineering, Czech Technical University in Prague, Prague, Czech Republic
[39] Faculty of Science, P.J. Šafárik University, Košice, Slovakia
[40] Frankfurt Institute for Advanced Studies, Johann Wolfgang Goethe-Universität Frankfurt, Frankfurt, Germany
[41] Fudan University, Shanghai, China
[42] Gangneung-Wonju National University, Gangneung, Republic of Korea
[43] Gauhati University, Department of Physics, Guwahati, India
[44] Helmholtz-Institut für Strahlen- und Kernphysik, Rheinische Friedrich-Wilhelms-Universität Bonn, Bonn, Germany
[45] Helsinki Institute of Physics (HIP), Helsinki, Finland
[46] High Energy Physics Group, Universidad Autónoma de Puebla, Puebla, Mexico
[47] Hiroshima University, Hiroshima, Japan
[48] Hochschule Worms, Zentrum für Technologietransfer und Telekommunikation (ZTT), Worms, Germany
[49] Horia Hulubei National Institute of Physics and Nuclear Engineering, Bucharest, Romania
[50] Indian Institute of Technology Bombay (IIT), Mumbai, India
[51] Indian Institute of Technology Indore, Indore, India
[52] Indonesian Institute of Sciences, Jakarta, Indonesia
[53] INFN, Laboratori Nazionali di Frascati, Frascati, Italy
[54] INFN, Sezione di Bari, Bari, Italy
[55] INFN, Sezione di Bologna, Bologna, Italy
[56] INFN, Sezione di Cagliari, Cagliari, Italy
[57] INFN, Sezione di Catania, Catania, Italy

[58] INFN, Sezione di Padova, Padova, Italy
[59] INFN, Sezione di Pavia, Pavia, Italy
[60] INFN, Sezione di Roma, Rome, Italy
[61] INFN, Sezione di Torino, Turin, Italy
[62] INFN, Sezione di Trieste, Trieste, Italy
[63] Inha University, Incheon, Republic of Korea
[64] Institute for Gravitational and Subatomic Physics (GRASP), Utrecht University/Nikhef, Utrecht, Netherlands
[65] Institute for Nuclear Research, Academy of Sciences, Moscow, Russia
[66] Institute of Experimental Physics, Slovak Academy of Sciences, Košice, Slovakia
[67] Institute of Physics, Homi Bhabha National Institute, Bhubaneswar, India
[68] Institute of Physics of the Czech Academy of Sciences, Prague, Czech Republic
[69] Institute of Space Science (ISS), Bucharest, Romania
[70] Institut für Kernphysik, Johann Wolfgang Goethe-Universität Frankfurt, Frankfurt, Germany
[71] Instituto de Ciencias Nucleares, Universidad Nacional Autónoma de México, Mexico City, Mexico
[72] Instituto de Física, Universidade Federal do Rio Grande do Sul (UFRGS), Porto Alegre, Brazil
[73] Instituto de Física, Universidad Nacional Autónoma de México, Mexico City, Mexico
[74] iThemba LABS, National Research Foundation, Somerset West, South Africa
[75] Jeonbuk National University, Jeonju, Republic of Korea
[76] Johann-Wolfgang-Goethe Universität Frankfurt Institut für Informatik, Fachbereich Informatik und Mathematik, Frankfurt, Germany
[77] Joint Institute for Nuclear Research (JINR), Dubna, Russia
[78] Korea Institute of Science and Technology Information, Daejeon, Republic of Korea
[79] KTO Karatay University, Konya, Turkey
[80] Laboratoire de Physique des 2 Infinis, Irène Joliot-Curie, Orsay, France
[81] Laboratoire de Physique Subatomique et de Cosmologie, Université Grenoble-Alpes, CNRS-IN2P3, Grenoble, France
[82] Lawrence Berkeley National Laboratory, Berkeley, California, United States
[83] Lund University Department of Physics, Division of Particle Physics, Lund, Sweden
[84] Moscow Institute for Physics and Technology, Moscow, Russia
[85] Nagasaki Institute of Applied Science, Nagasaki, Japan
[86] Nara Women's University (NWU), Nara, Japan
[87] National and Kapodistrian University of Athens, School of Science, Department of Physics , Athens, Greece
[88] National Centre for Nuclear Research, Warsaw, Poland
[89] National Institute of Science Education and Research, Homi Bhabha National Institute, Jatni, India
[90] National Nuclear Research Center, Baku, Azerbaijan
[91] National Research Centre Kurchatov Institute, Moscow, Russia
[92] Niels Bohr Institute, University of Copenhagen, Copenhagen, Denmark
[93] Nikhef, National institute for subatomic physics, Amsterdam, Netherlands
[94] NRC Kurchatov Institute IHEP, Protvino, Russia
[95] NRC «Kurchatov»Institute - ITEP, Moscow, Russia
[96] NRNU Moscow Engineering Physics Institute, Moscow, Russia
[97] Nuclear Physics Group, STFC Daresbury Laboratory, Daresbury, United Kingdom
[98] Nuclear Physics Institute of the Czech Academy of Sciences, Řež u Prahy, Czech Republic
[99] Oak Ridge National Laboratory, Oak Ridge, Tennessee, United States
[100] Ohio State University, Columbus, Ohio, United States
[101] Petersburg Nuclear Physics Institute, Gatchina, Russia
[102] Physics department, Faculty of science, University of Zagreb, Zagreb, Croatia
[103] Physics Department, Panjab University, Chandigarh, India
[104] Physics Department, University of Jammu, Jammu, India
[105] Physics Department, University of Rajasthan, Jaipur, India
[106] Physikalisches Institut, Eberhard-Karls-Universität Tübingen, Tübingen, Germany
[107] Physikalisches Institut, Ruprecht-Karls-Universität Heidelberg, Heidelberg, Germany
[108] Physik Department, Technische Universität München, Munich, Germany
[109] Politecnico di Bari and Sezione INFN, Bari, Italy
[110] Research Division and ExtreMe Matter Institute EMMI, GSI Helmholtzzentrum für Schwerionenforschung GmbH, Darmstadt, Germany

[111] Russian Federal Nuclear Center (VNIIEF), Sarov, Russia
[112] Saha Institute of Nuclear Physics, Homi Bhabha National Institute, Kolkata, India
[113] School of Physics and Astronomy, University of Birmingham, Birmingham, United Kingdom
[114] Sección Física, Departamento de Ciencias, Pontificia Universidad Católica del Perú, Lima, Peru
[115] St. Petersburg State University, St. Petersburg, Russia
[116] Stefan Meyer Institut für Subatomare Physik (SMI), Vienna, Austria
[117] SUBATECH, IMT Atlantique, Université de Nantes, CNRS-IN2P3, Nantes, France
[118] Suranaree University of Technology, Nakhon Ratchasima, Thailand
[119] Technical University of Košice, Košice, Slovakia
[120] The Henryk Niewodniczanski Institute of Nuclear Physics, Polish Academy of Sciences, Cracow, Poland
[121] The University of Texas at Austin, Austin, Texas, United States
[122] Universidad Autónoma de Sinaloa, Culiacán, Mexico
[123] Universidade de São Paulo (USP), São Paulo, Brazil
[124] Universidade Estadual de Campinas (UNICAMP), Campinas, Brazil
[125] Universidade Federal do ABC, Santo Andre, Brazil
[126] University of Cape Town, Cape Town, South Africa
[127] University of Houston, Houston, Texas, United States
[128] University of Jyväskylä, Jyväskylä, Finland
[129] University of Kansas, Lawrence, Kansas, United States
[130] University of Liverpool, Liverpool, United Kingdom
[131] University of Science and Technology of China, Hefei, China
[132] University of South-Eastern Norway, Tonsberg, Norway
[133] University of Tennessee, Knoxville, Tennessee, United States
[134] University of the Witwatersrand, Johannesburg, South Africa
[135] University of Tokyo, Tokyo, Japan
[136] University of Tsukuba, Tsukuba, Japan
[137] Université Clermont Auvergne, CNRS/IN2P3, LPC, Clermont-Ferrand, France
[138] Université de Lyon, CNRS/IN2P3, Institut de Physique des 2 Infinis de Lyon , Lyon, France
[139] Université de Strasbourg, CNRS, IPHC UMR 7178, F-67000 Strasbourg, France, Strasbourg, France
[140] Université Paris-Saclay Centre d'Etudes de Saclay (CEA), IRFU, Départment de Physique Nucléaire (DPhN), Saclay, France
[141] Università degli Studi di Foggia, Foggia, Italy
[142] Università di Brescia, Brescia, Italy
[143] Variable Energy Cyclotron Centre, Homi Bhabha National Institute, Kolkata, India
[144] Warsaw University of Technology, Warsaw, Poland
[145] Wayne State University, Detroit, Michigan, United States
[146] Westfälische Wilhelms-Universität Münster, Institut für Kernphysik, Münster, Germany
[147] Wigner Research Centre for Physics, Budapest, Hungary
[148] Yale University, New Haven, Connecticut, United States
[149] Yonsei University, Seoul, Republic of Korea